THESIS FOR THE DEGREE OF DOCTOR OF PHILOSOPHY

Wood xylan and modified xylan

Solubilization, film formation and water interactions

CHONNIPA PALASINGH

Department of Chemistry and Chemical Engineering

CHALMERS UNIVERSITY OF TECHNOLOGY

Gothenburg, Sweden 2022

Wood xylan and modified xylan

Solubilization, film formation and water interactions

CHONNIPA PALASINGH
ISBN 978-91-7905-733-6

Doktorsavhandlingar vid Chalmers tekniska högskola
Ny serie nr 5199
ISSN 0346-718X

Department of Chemistry and Chemical Engineering
Chalmers University of Technology
SE-412 96 Gothenburg
Sweden
Telephone + 46 (0)31-772 1000

Cover:
An illustration of modified wood xylan, its solubility and a thin film.

Printed by Chalmers digitaltryck
Gothenburg, Sweden 2022

Wood xylan and modified xylan

Solubilization, film formation and water interactions

CHONNIPA PALASINGH
Department of Chemistry and Chemical Engineering
Chalmers University of Technology

ABSTRACT

Wood xylans are biopolymers that are valuable for future materials and renewable engineering solutions. In this study, xylan solubility in polar solvents and film formation were investigated. Most wood xylans are poorly soluble in polar solvents, such as water, and this can be a critical hindrance for facilitating new uses of xylan, especially in solution-based processes. Modification via oxidation using sodium periodate was selected as a potential prospect to improve xylan solubility. The influence of modification, such as the degree of oxidation, was investigated using solutions and thin films. Surface-sensitive analytics were used to quantify the properties of modified xylan as films and film additives, with a focus on their interaction with water. Furthermore, a correlation between film morphology and material solubility of modified xylan and unmodified xylan in blend systems was observed using atomic force microscopy. The findings expand the possibility of utilizing wood xylan in solution-based processes.

Keywords: polysaccharide, periodate oxidation, adsorption, thin film

LIST OF PUBLICATIONS

This thesis is based on the work contained in the following Papers:

I. **Modification of xylan via an oxidation–reduction reaction**
Chonnipa Palasingh, Koyuru Nakayama, Felix Abik, Kirsi S. Mikkonen, Lars Evenäs, Anna Ström and Tiina Nypelö
Carbohydrate Polymers 292(2022): 119660.

II. **Morphology and swelling of thin films from dialcohol xylan**
Chonnipa Palasingh, Rupert Kargl, Karin Stana Kleinschek, Jana Schaubeder, Stefan Spirk, Anna Ström and Tiina Nypelö
Manuscript.

III. **Lignin – xylan blend phase separation in thin films**
Panagiotis Spiliopoulos, **Chonnipa Palasingh,** Caterina Czibula, Christian Teichert, and Tiina Nypelö
Manuscript.

IV. **Design of friction, morphology, wetting, and protein affinity by cellulose blend thin film composition**
Caterina Czibula, Gundula Teichert, Maximilian Nau, Mathias Hobisch, **Chonnipa Palasingh**, Markus Biesalski, Stefan Spirk, Christian Teichert, and Tiina Nypelö
Frontiers in Chemistry 7(2019), article number: 239.

V. **Oxidized xylan additive for nanocellulose films—a swelling modifier**
Chonnipa Palasingh, Anna Ström, Hassan Amer, and Tiina Nypelö
International Journal of Biological Macromolecules 180(2021): 753–759.

CONTRIBUTION REPORT TO LISTED PUBLICATIONS

I. Planned experiments with coauthors and performed all experiments except for size-exclusion chromatography measurements. Wrote the first draft of the manuscript. Main author.

II. Planned experiments with coauthors and performed all experiments except for dynamic light scattering measurements. Wrote the first draft of the manuscript. Main author.

III. Responsible for xylan incorporation into thin films. Performed part of the atomic force microscopy measurements and data processing. Coauthor.

IV. Co-performed quartz crystal microbalance with dissipation monitoring experiments. Coauthor.

V. Planned experiments with the coauthors and performed all experiments. Wrote the first draft of the manuscript. Main author.

PUBLICATIONS NOT INCLUDED IN THIS THESIS

Video speed switching of plasmonic structural colors with high contrast and superior lifetime
Kunli Xiong, Oliver Olsson, Justas Svirelis, **Chonnipa Palasingh**, Jeremy Baumberg, and Andreas Dahlin
Advanced Materials 33.41(2021): 2103217.

Current opportunities and challenges in biopolymer thin film analysis—determination of film thickness
Spirk, Stefan, **Chonnipa Palasingh**, and Tiina Nypelö
Frontiers in Chemical Engineering 2021(2021): 755446.

Wood hemicelluloses and derivates at interfaces - towards use in food and feed
Felix Abik, **Chonnipa Palasingh**, Mamata Bhattarai, Shaun Leivers, Anna Ström, Bjørge Westereng, Kirsi S. Mikkonen, Tiina Nypelö
Manuscript.

ABBREVIATIONS

AFM	Atomic force microscopy
AXU	Anhydroxylose unit
CNF	Cellulose nanofiber
DalX	Dialcohol xylan
DAX	Dialdehyde xylan
D_h	Hydrodynamic diameter
DMSO	Dimethyl sulfoxide
DO	Degree of oxidation
HPCE	Hydroxypropyl cellulose stearate
NMR	Nuclear magnetic resonance
QCM-D	Quartz crystal microbalance with dissipation monitoring
SPR	Surface plasmon resonance
TCNF	TEMPO-oxidized cellulose nanofiber
TEMPO	2,2,6,6-tetramethyl-1-piperidinyloxy
TMSC	Trimethylsilyl cellulose

CONTENTS

1
INTRODUCTION

Wood is a renewable natural material that stores carbon dioxide during growth and has been explored as a potential resource for replacing fossil-based products. Even though a consumption of wood has increased to almost 4 billion m^3 in 2018, the global forest area has remained rather constant over past three decades [1]. The development of technology, manufacturing innovation, and a circular economy are the top priorities in wood research.

At the beginning of human civilization, wood was used in its original form to build, create tools, and for fuel. The advancement of knowledge and technology led to more elaborate wood processing, which enabled even wider utilization in various fields, such as the manufacture of chemicals, materials, and energy from wood components.

Cellulose, hemicelluloses, and lignins are macromolecules extracted from wood. These resources are attractive alternatives to fossil-based materials. Cellulose and its derivatives are widely used in paper products [2, 3], cosmetics [4], pharmaceuticals [5], medical [6], and textiles [7]. Lignins have applications as a starting material for the production of fine chemicals, phenol derivatives, biofuels, and carbon fibers [8]. Hemicelluloses from wood—xylan, for example—have the potential for use as additives, coatings, and stabilizers [9].

Hemicelluloses have been used in cellulose products. They are present in cellulose fibers and have enhanced strength and flexibility [10-12]. Hemicelluloses, such as xylan [13], arabinoxylan [14], xyloglucan [15], and glucuronoxylan [11], have demonstrated applications for tuning cellulose film properties through adsorption. However, the xylan market is small, perhaps because of the lack of efficient extraction and purification

technology that would simultaneously facilitate cost efficiency. This further hinders product development and commercial use.

This research focuses on the solubilization of xylan in polar solvents, specifically the impact of molecular composition and periodate oxidation on xylan dispersion and film formation. Xylan modification via periodate oxidation and sodium borohydride reduction is presented in Paper I. Modification of xylan was performed to extend its solubility and promote solvent interactions. Modification with sodium periodate alters the backbone structure of xylan by cleaving the carbon bond between C2 and C3 of xylopyranose units [16]. The modified grades were formed into films in Paper II. The interactions of the films with humid air were revealed using surface-sensitive analytics: quartz crystal microbalance with dissipation monitoring (QCM-D). The concept of solubility was taken further, and xylans and lignins were combined in a solution and transformed into blend films patterned by phase separation in Paper III. In Paper IV, blend films, this time from cellulose derivatives, were demonstrated with a combination of surface-sensitive analysis, QCM-D, and surface plasmon resonance (SPR) spectroscopy. Modified xylans were applied to cellulose surfaces, and their water uptake was elucidated with a combination of surface-sensitive analytics in Paper V.

2
BACKGROUND

This chapter provides the background of the characteristics of wood-based polymers, their modification, the thin films thereof, and their characterization.

2.1 Wood polysaccharides

Wood cell wall consists of several layers with distinct chemical composition and arrangement. They contain an assembly of cellulose, hemicelluloses and lignins which can be divided into two categories: polysaccharides and aromatic compounds [17, 18]. Cell wall composition and properties depend on the species and type of wood. In general, hardwoods consist of 40–44% cellulose, 15–35% hemicelluloses, and 18–25% lignin, while softwoods contain more hemicelluloses (30–32%) and lignins (25–32%) [19]. In addition to these three major components, a small amount of extractives, pectin, and inorganic compounds can be found in wood. Pulping is a process used to separate fiber from other components of wood. The process involves either chemical, mechanical, or combined methods to fractionate the wood components. Chemical pulping primarily uses chemicals like sulfates and caustic soda in combination with heat to remove lignin and mechanical refining to separate fibers, while mechanical pulping usually requires pretreatment—for example, with steam—prior to mechanical grinding or refining. Additional processes such as screening, bleaching, and purification may also be used [18].

Wood polysaccharides: the backbones of cellulose and hemicelluloses contain one or more kinds of repeating monosaccharides. Glucopyranose, mannopyranose, xylopyranose, galactopyranose, and arabinopyranose are common monosaccharides found in wood cell walls, with the first three typically found as backbone units [17]. Cellulose is a linear homopolysaccharide consisting of β-1,4-glycosidic-linked

glucopyranose units (Figure 1). Cellulose molecules align to form semi-crystalline microfibrils. Bundles of microfibrils are the central structural units in plant fibers [17, 20, 21].

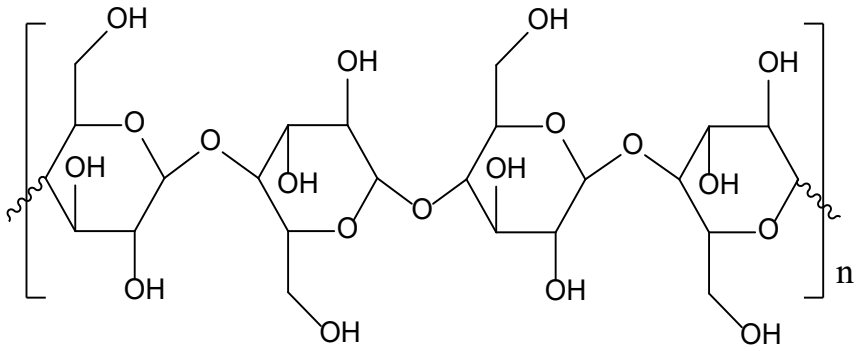

Figure 1. Chemical structure of cellulose showing the β-1,4 glycosidic linked glucopyranose units

Hemicelluloses in wood are found in a matrix between cellulose microfibrils in the cell walls [18]. They are generally shorter than cellulose with a degree of polymerization between 80 and 200 [22, 23]. Hemicelluloses are composed of one or more monosaccharides that are arranged into a linear backbone, with or without branched substitutions. Monosaccharides such as mannopyranose, xylopyranose, glucopyranose, arabinopyranose, and galactopyranose are found in wood hemicelluloses [17, 22-24]. Uronic acids and acetyl groups can also be found as substituents [23, 25]. Wood hemicelluloses are divided into two main categories: mannans and xylans. The former group comprises mannopyranose, and glucopyranose, backbone units, while the latter mainly contains xylopyranose units. Composition of hemicelluloses is difference in softwood and hardwood. Softwood hemicelluloses contain a larger portion of mannopyranose and galactopyranose but lower acetyl groups than that of hardwood [21].

Xylan is typically a linear polysaccharide consisting of β-1,4-glycosidic-linked xylopyranose units (Figure 2). Xylan is a hemicellulose found in hardwoods (10–35%) and softwoods (10–15%) [21, 23].

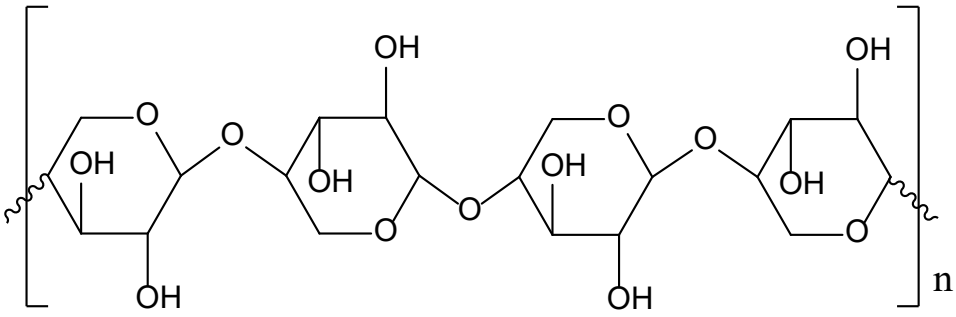

Figure 2. Chemical structure of xylan showing β-1,4 glycosidic linked xylopyranose units

2.2 Solubility of xylan

Solubility is the ability of a substance to dissolve in a solvent at a specific temperature [26]. Dissolution relates to fundamental thermodynamics based on entropy (S) and enthalpy (H) at a particular temperature (T) (Equation 1). Homogeneous solutions require a net energy, called Gibbs free energy (G), to be negative. Unlike small molecules, each polymer segment cannot move freely, which greatly influences S. Solubility depends on inter- and intramolecular bonding, the stiffness of the polymer backbone, and its long-range order. Polymers often face solubility problems because of their high molar mass, which results in small S gains upon dissolution [27]. In some cases, energy is injected through heating to lower ΔG of the system and to promote dissolution.

$$\Delta G = \Delta H - T\Delta S \quad (1)$$

The solubility of xylan is governed by its physicochemical properties: monosaccharide composition, branching, conformation, type of substituted groups, and molar mass. Abundant hydroxyl groups on xylan can be expected to have affinity to water; however, xylans have been observed to aggregate in water, indicating that they also have high affinity to themselves [28, 29]. Dissolution will occur when xylan prefers to interact with the solvent, such as water, rather than with itself, or there are certain factors such as branching that prevent xylan–xylan interactions [24, 30].

Neutral and charged (such as uronic acid) side groups interrupt the conformation due to steric and electrostatic repulsion, respectively. Both of which promote xylan-solvent interaction. For example, water-soluble arabinoxylan became insoluble after removing most of arabinose side groups (0.04 arabinose to xylose ratio) [31].

Acetylation was found to greatly affect solubility as fully acetylated glucuronoxylan dissolved in chloroform and dimethyl sulfoxide (DMSO), while the non-acetylated glucuronoxylan did not [32].

Molar mass is another factor that governs dissolution. The larger molecule has a tendency to promote self-interaction, which will decrease solubility [33]. Molar mass may increase upon storing due to aggregation, as demonstrated for arabinoxylan [34].

2.3 Periodate oxidation of xylan

Periodate oxidation was introduced for the analysis of polysaccharides [35]. Later, it was used for preparative purposes [36, 37]. This oxidation involves regioselective cleavage of the carbon–carbon bond between C2 and C3 of a monosaccharide unit and leads to the formation of aldehydes at those sites. The reactive aldehyde groups can transform into hydrated aldehyde and form hemiacetal or hemialdal linkages in an aqueous environment (Figure 3). In addition, they can act as intermediates for further modification, where aldehydes react with other moieties, such as cationic Girard's reagent [38], methyl and butyl amine [39] and p-toluidine [40] for specific functionality.

Side reactions, such as the peeling reaction and free radical depolymerization, may occur during the oxidation, which is experienced not only by xylan [41] but also by other polysaccharides, such as cellulose [42], chitosan [43], and alginate [44]. The peeling reaction takes place at reducing ends and newly generated reducing ends, which are a result of glycosidic bond cleavage [45, 46]. Unwanted radicals are generated in the presence of light and impurities, such as lignins or proteins [45]. Radical formation can be prevented by adding a radical scavenger, for example, isopropanol [45, 46].

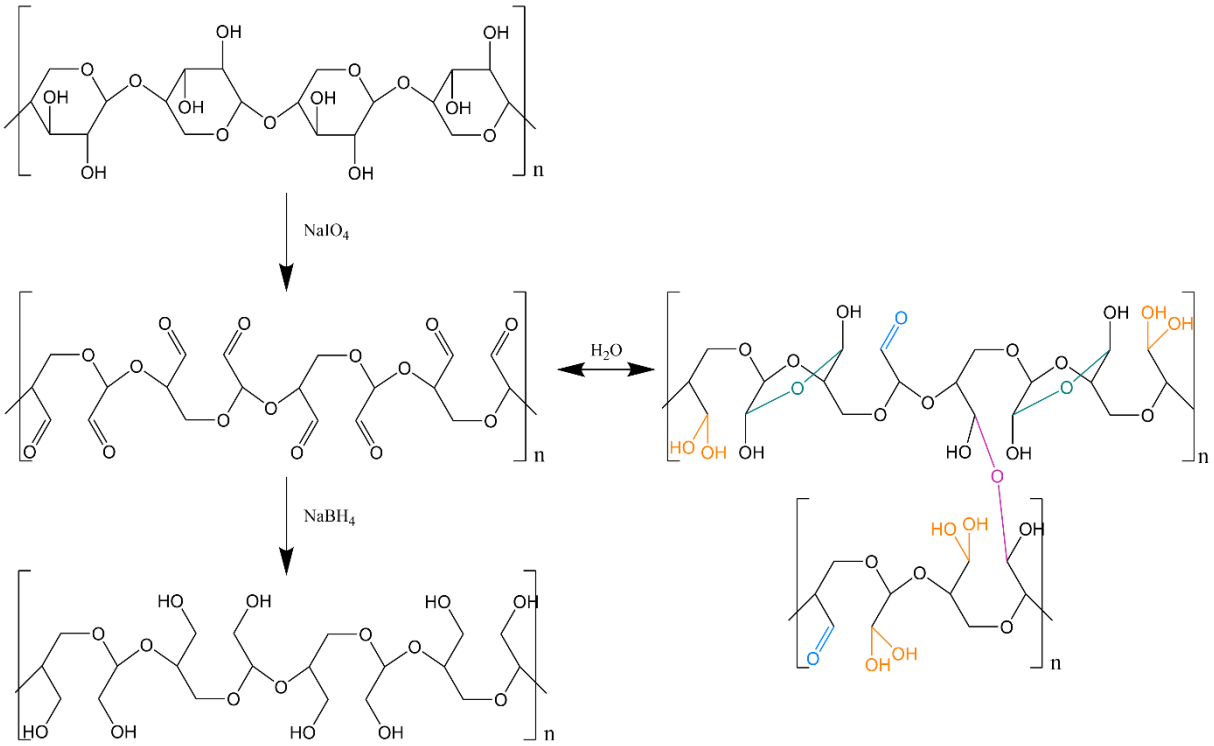

Figure 3. Periodate oxidation and borohydride reduction of xylan to dialdehyde xylan and dialcohol xylan, respectively, with possible conformation of dialdehyde xylan in water. Free aldehyde (blue), hydrated aldehyde (orange), hemialdal linkage (green), hemiacetal linkage (magenta)

2.4 Thin films

Polysaccharide thin films have been explored over past decades for electronic [47], pharmaceutical [48], medical [49], and material [50, 51] applications and analytical purposes [52]. A thin film refers to a film that is thinner than 100 nm and is often deposited on a support, such as a silicon wafer [53]. Thin films can be divided into two categories: open films and closed films. Open films are noncontinuous films that consist of regions of the coating substance on a substrate, while closed films have full coverage on a substrate. The closed films have been used for analytical purposes, such as studying surface energy, enzymatic activity [54], swelling and deswelling [50, 55, 56], and adsorption [57].

The films can be manufactured using dipping, spinning, or spraying techniques, such as Langmuir-Blodgett, Langmuir-Schaefer, spin coating, and spray coating [58]. Spin coating was used in this thesis for the preparation of thin films. It is a solution-based

technique that involves dissolution or dispersion of polysaccharides in a volatile solvent [59]. The fundamental of spin coating involves the high-speed rotation of a substrate, which leads to deposition of a thin film onto the substrate (Figure 4). A small amount of a solution is dispensed onto a substrate. When the spinning begins, excess liquid is cast off, and the solvent evaporates, leaving behind a layer of the nonvolatile material. The film thickness is influenced by solute concentration and spinning parameters, such as rotational speed and acceleration [60]. Since solubility is often required for film deposition, polysaccharides are derivatized into their soluble counterparts. Nanosized colloidal dispersion can also be spin coated into films, and in the case of less volatile solvents, heat can be applied to aid in evaporation of the solvent [59].

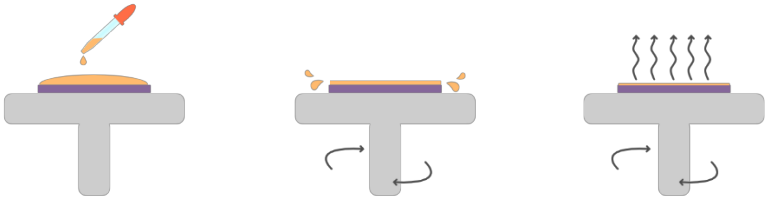

Figure 4. Spin-coating process. Solution is added onto a substrate as the spinning starts, and excess solution is cast off due to the rotational motion. The solvent evaporates and leaves behind the nonvolatile material deposited on the substrate

Patterned thin films have been used in advanced applications, such as in pharmaceutics, electronics, and biotechnology. Bio-based patterned films have been used in drug delivery [61, 62], for coating electronics [51], and for the immobilization of DNA [63]. One option for creating patterned thin films is to use a multicomponent solution that contains, for example, two polymers that will phase separate when the solvent is evaporated and the concentration increases. The pattern of phase separation depends on the solubility and miscibility of the polymers, volume fraction, substrate, and spin-coating speed and acceleration [61]. During spin coating, the solvent evaporates, which rapidly increases the concentration of the polymers and leads to a structure forming. The phase separation phenomenon has been described via a metastable and unstable state in the two-phase region (Figure 5) [61, 62]. Nucleation and growth and spinodal decomposition are two-phase-separation mechanisms in the meta- and unstable regions (Figure 5). In the metastable region, features are created from nuclei forming and growing. In the

unstable region, the rapid fluctuation of polymer concentration develops into a percolation-to-cluster transition.

Hydrodynamic growth, coalescence, and Ostwald ripening are coarsening mechanisms that may further define the evolution of the structures during spinning. Hydrodynamic growth is driven by Laplace pressure, which is a pressure difference between the inside and outside of a curved surface at an interface of two immiscible liquids, caused by surface tension at the interface [64]. This moves liquid from the high curve toward the lower curve, which is a flow from a small branch toward a larger connecting branch. The merging of two droplets is called coalescence [65], while in Oswald ripening, where small droplets combine and form a larger droplet [66].

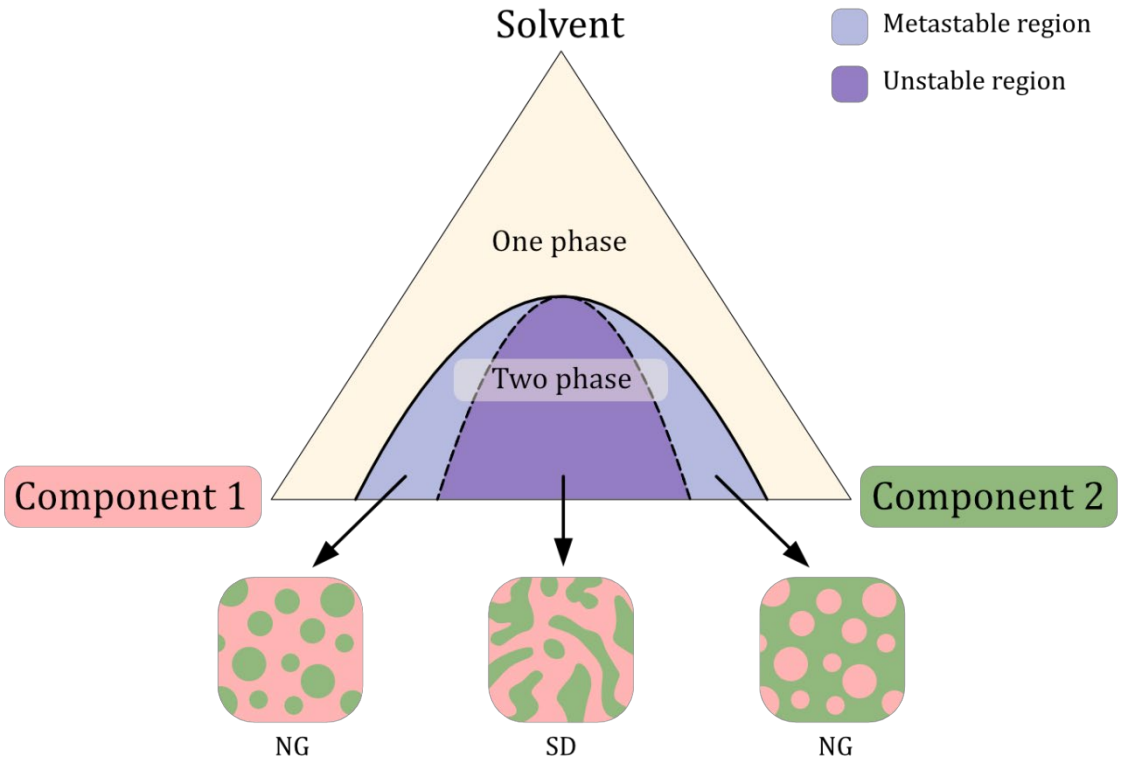

Figure 5. Phase diagram of a three-component system. One phase separates into two phases via nucleation and growth (NG) in the metastable region and spinodal decomposition (SD) in the unstable region

2.5 Adsorption on solid substrate

Adsorption at an interface refers to an increase in the concentration of a solute at the interfacial region [67]. If adsorption involves forming a chemical bond between the solute and the surface, the process is called chemisorption. Physisorption involves physical interaction, such as van der Waals interactions. The adsorption is driven primarily by free energy associated with the interactions of the solute (polymer segments), the solvent, and the surface. Both poor interaction between polymer segments and a solvent and strong affinity between the polymer segments and the surface promote adsorption. Polymer adsorption involves the diffusion of polymers to interfacial regions, attachment of the polymer segments to the surface, and the rearrangement of the segments on the surface (Figure 6). In a good solvent, solute is adsorbed less at the interface, compared to a theta solvent, because the polymer segments have a high affinity toward the solvent [67]. The adsorbed polymer behaves differently in a different solvent environment; for example, solute tends to extend in a good solvent, which means that it will occupy more space [67, 68]. A higher molar mass solute is more prone to adsorb on the surface because it is less stable in the solution compared to lower molar mass solutes [68]. In high dispersity solutions, such as is the case often for xylan, which contains various lengths of chains, short chains move faster and reach the surface first, then adsorb and rearrange. Longer chains, which reach the surface later, have a high tendency to replace small molecules on the surface because of the larger entropy gain they induce upon adsorption. This causes high dispersity species to take a longer time to reach a plateau in the adsorbed amount [67].

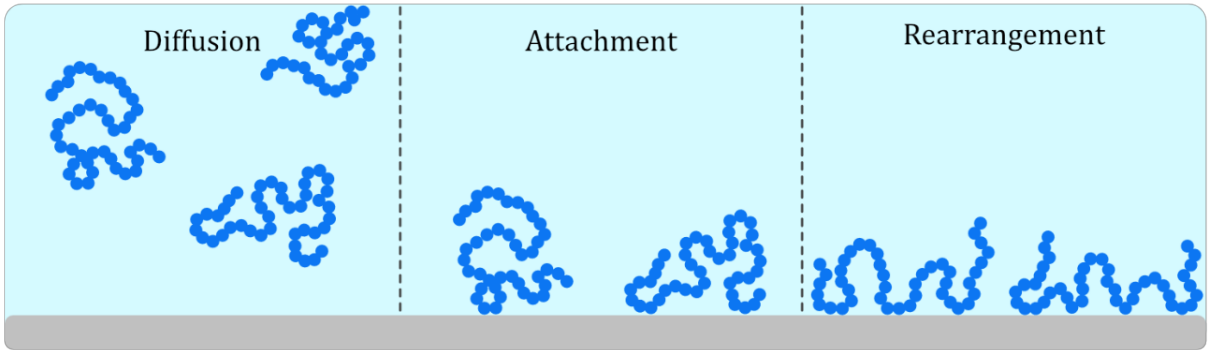

Figure 6. Schematic presentation of a polymer adsorbing on a solid surface. Blue chains represent the polymers/high molar mass solutes in an aqueous environment

The charge of the surface or the polymer solute has an influence on the interaction between polymer segments and the surface. Oppositely charged species are attracted via Coulombic attraction, and polymers may then adsorb on the surface (Figure 7a). When adsorption occurs, counter ions are released and an increase in entropy is obtained (lower the energy of the system). On the other hand, in polymers and surfaces with the same charge, the driving forces are van der Waals between the polymer segments and surface or hydrophobic effects (Figure 7b).

Temperature, pH, type of salt, charge density, and ionic strength are other factors that can promote or hinder adsorption. For instance, the high charge density of polymers that have opposite charges to a surface, up to a certain charge density, will promote adsorption to the surface. However, too high a charge density will slowly decrease the total adsorbed amount because the polymers tend to rearrange at the surface in a flat conformation, which increases the space occupied on the surface [67]. For adsorption in thin film, film mass or thickness is a crucial factor for adsorption analysis, since some properties. such as swelling, greatly depend on thickness or film mass, especially for hydrophilic materials.

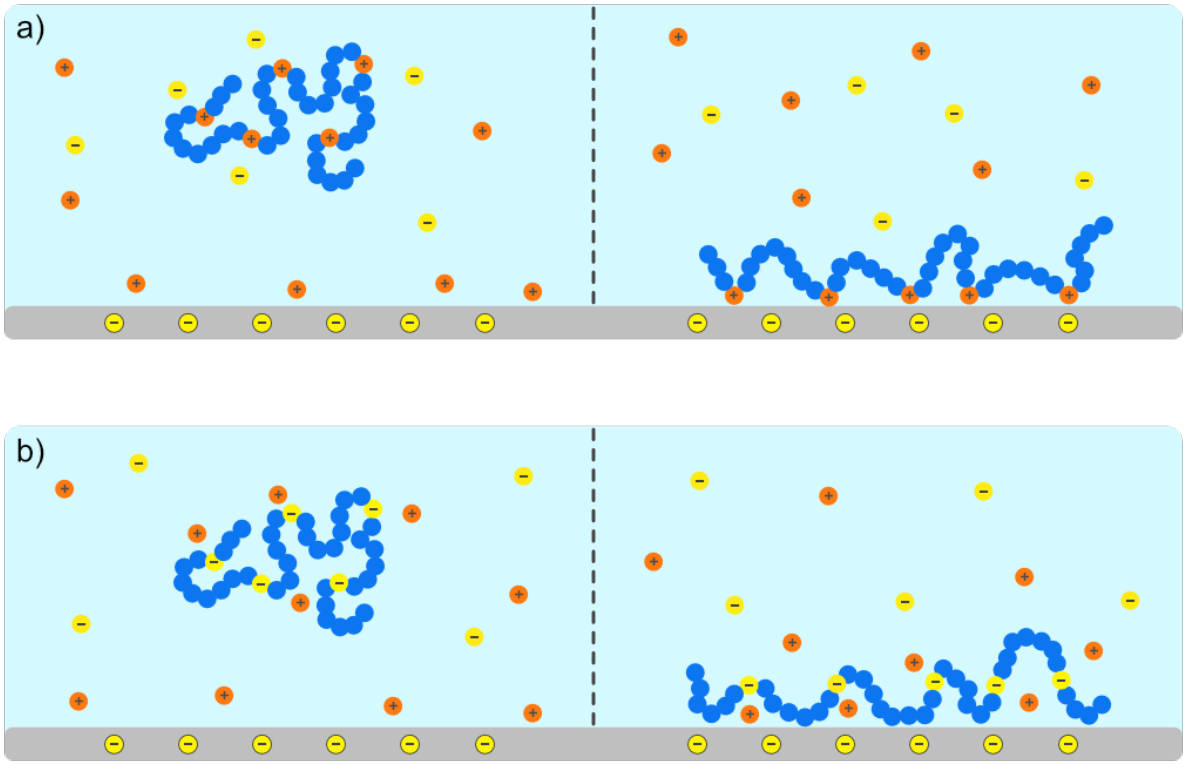

Figure 7. Adsorption of (a) charged polymers on opposite charged surface and (b) charged polymers on a surface with the same charge

2.6 Surface-sensitive analytical techniques

Quartz crystal microbalance with dissipation monitoring (QCM-D) and surface plasmon resonance (SPR) spectroscopy were employed in the work for this thesis to determine thickness, swelling, and adsorption on thin films. These techniques enable real-time monitoring with nanoscale resolution and a label-free environment. However, they are complimentary in terms of which physical quantity is tracked and, consequently, what information can be obtained from the experiment. These two techniques have been used in several fields, such as biology, chemistry, medicine, and material science [69-71].

QCM-D is a precise balance with sensitivity on a nanogram scale. A principle of QCM-D lies in the oscillating resonance of the sensor, which is generated by applying voltage to the sensor. The resonance frequency, which depends on mass attached to a surface, is monitored as a function of time. A change in frequency (Δf) indicates a mass change on the sensor surface, which is useful in quantifying many phenomena, such as molecules binding or desorbing from a surface (Figure 8a). Energy dissipation (E_d) is a way to determine the energy losses in the system. Dissipation (D) is defined as E_d per oscillation divided by energy stored (E_s) (Equation 2), where D increases when the layer is soft or thick or liquid is present in it (Figure 8b). Note that the soft layer refers to a layer that exhibits viscous characteristics, such as is common for polymers and biomolecules.

$$D = \frac{E_d}{2\pi E_s} \tag{2}$$

The Sauerbrey model is the simplest model for analysis of QCM-D experimental data. The mass change (m) is calculated through the relationship between overtone (n), crystal sensitivity (C), and recorded frequency change (Δf) (Equation 3). Note that C is constant (0.177 mg/m^{2}Hz) and n values are 1, 3, 5, …, 13. Most polysaccharide films are viscoelastic, and as the Sauerbrey equation does not account for viscoelasticity, it cannot give an accurate value. However, it is used for estimation and convenience [72].

$$m = -C\frac{\Delta f}{n} \tag{3}$$

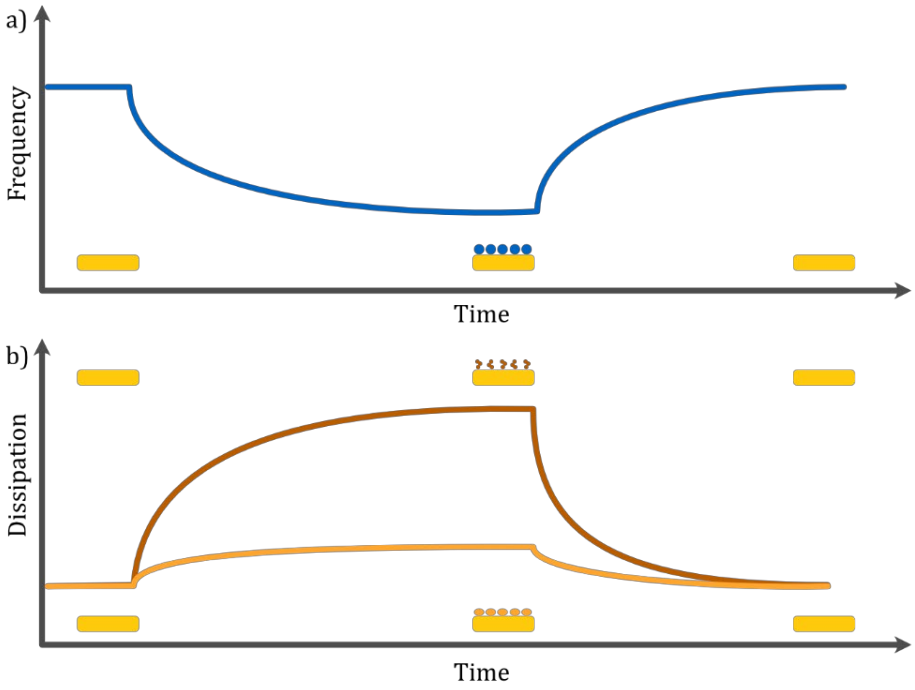

Figure 8. QCM-D configuration (a) frequency change as a function of time, as molecules adsorb or desorb from the surface and (b) dissipation response of soft (brown) and rigid (yellow) layer deposition and immigration from surface

Johannsmann et al. [73] derived a model that included the viscoelastic property of a material (Equation 4). This model is used under the assumption that complex shear compliance ($\hat{\jmath}(f)$) is independent of frequency in the experimental range [72]. A true sensed mass (m^0), which refers to mass change on the sensor surface, is obtained from the interception of a linear regression of an equivalent mass ($\hat{m}^*$) against the resonance frequency square (f^2).

$$\hat{m}^* = m^0\left(1 + \hat{\jmath}(f)\frac{\rho f^2 d^2}{3}\right) \tag{4}$$

Note that ρ is the density of fluid and d is the film thickness.

SPR spectroscopy is another surface-sensitive technique that relies on the plasmon phenomenon and refractive index of the material. In the Kretschmann configuration (Figure 9a), polarized light travels through a prism and hits the backside of a metal layer, which is commonly gold. When electrons on the metal layer absorb at specific wavelengths of light, get excited, and oscillate, this is a phenomenon called “plasmon resonance.” Those excited electrons create an electromagnetic field called an “evanescent

field," which is sensitive to the environment. SPR spectroscopy uses this principle to detect materials adsorbed or desorbed from a surface within the evanescent field, a few hundred nanometers perpendicular to the surface [74]. There are two visual information that are gathered from the SPR response of the angular scan (Figure 9b): total internal reflection angle and minimum intensity angle. The total internal reflection angle is the angle at which the metal layer acts like a mirror and totally reflects light, which is under the influence of the refractive index of the bulk medium. In contrast, the minimum intensity angle is an angle where the metal layer totally absorbs light. The angle depends on the refractive index of the molecules bound to the surface. Kinetics at the surface can be obtained through a continuous angular scan by observing the minimum intensity angle over time (Figure 9c).

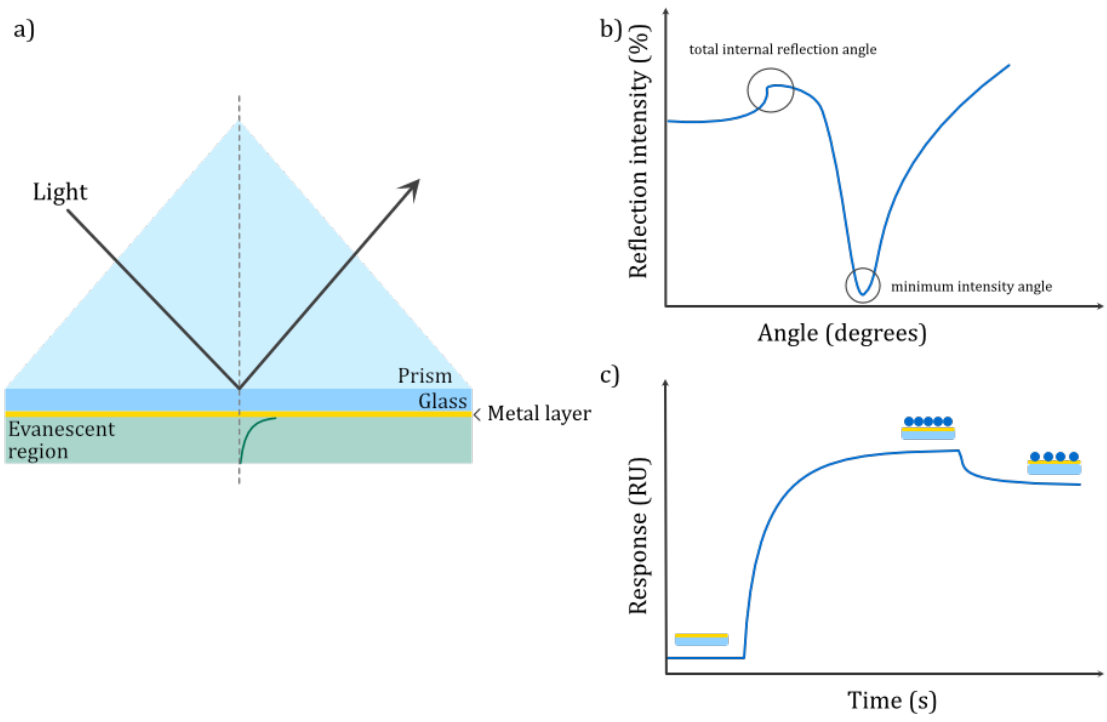

Figure 9. SPR spectroscopy (a) Kretschmann configuration, (b) angular scan (c) and an SPR sensorgram of molecules binding on a surface

Adsorbed mass on a surface can be calculated through the modified de Feijter equation (Equation 5), where $\Delta\theta$ is a shift of the minimum intensity angle obtained from two separated angular scans for ex situ deposition or from response from continuous scan for in situ adsorption/desorption, k is a sensitivity constant of SPR, d_p is a thickness of adsorbed layer, and dn/dc is a refractive index increment.

$$\Gamma = \frac{\Delta\theta k d_p}{\frac{dn}{dc}} \quad (5)$$

Note that adsorbed mass extracted from SPR spectroscopy is only the mass of the material that was bound to a surface, while the mass extracted from QCM-D is the mass of the materials with solvent coupling. This is because QCM-D works like a balance and does not differentiate solute and solvent molecules [75].

3

EXPERIMENTAL

3.1 Polysaccharide modification

Xylans were modified via oxidation or oxidation and reduction (Papers I, II, and V). The oxidation procedure was adopted from Amer et al. [16]. First, 4 g of xylan was dispersed in 115 ml of water overnight before adding 10 ml of isopropanol, and then the flask was covered with aluminum foil. In Paper II, the solution was heated to 70 °C for 30 min and cooled to room temperature before the reaction was initiated. The periodate solution was shielded from light during the dissolution of sodium periodate in 75 ml water. The reaction was initiated by adding the periodate solution into the xylan solution and was stirred for 24 h, except Paper V, where the reaction was allowed to continue for 96 h. The reaction was performed in the absence of light and at room temperature. In the case of producing dialdehyde xylan (DAX) (Paper V), the product was dialyzed against water for two days and was then freeze dried. In the case of dialcohol xylan (DalX), ethylene glycol was added to quench unreacted periodate in some batches, and then the grade was reduced with sodium borohydride. This solution was freshly prepared. The final products were purified by dialysis.

TEMPO-oxidized cellulose nanofiber (TCNF) which contained carboxylated groups was studied in Paper V. Catalyzed oxidation with 2,2,6,6-tetramethyl-1-piperidinyloxy (TEMPO) was performed by suspending 1 g of cellulose nanofibers (CNF) in a 100 ml solution that contained 0.1 mmol TEMPO and 1 mmol NaBr. Then 3.8 mmol of 12% NaClO solution (pH 10) was added. Oxidation was performed at room temperature. To maintain a pH of 10, 0.5 M NaOH was added dropwise until pH was stable, indicating that the

reaction finished. The TCNFs were purified by dialyzing in water again. The procedure was adapted from Saito et al. [76].

3.2 Carbohydrate composition

Acid hydrolysis was performed as guided by Theander and Westerlund in Papers I, II, and V [77]. To accomplish this, 30 mg of xylans and modified xylans were hydrolyzed with 0.45 ml 72% sulfuric acid under vacuum for 15 min followed by 1 h in a 30 °C water bath. The hydrolysates were diluted with 12.6 g of warm deionized water and placed in an autoclave at 125 °C for 1 h. The hydrolysates were filtered with a glass microfiber filter and diluted to 25 ml total volume with warm water. For analysis, 1 ml of diluted filtered hydrolysate was added to a 50 ml volumetric flask, followed by adding 2 ml of 200 mg/l fucose internal standard and then adjusting the volume to 50 ml with deionized water. The sample was filtered with a 0.2 μm syringe filter before analyzing with high-performance anion exchange chromatography with pulsed amperometric detection using a Dionex ICS 3000 ion chromatography system equipped with a CarboPac™ PA1 analytical column. In Paper V, the preparation procedure was slightly adapted from the previous method, wherein a fritted glass crucible was used instead of a glass filter.

3.3 Molar mass of xylans and their derivatives

In Papers I and II, molar mass was determined using size-exclusion chromatography. Xylans and DalXs were dissolved in 0.01 M LiBr/DMSO at a concentration of 2 mg/ml. For some of the grades, pre-swelling with 30 μl water overnight was required before adding LiBr/DMSO solvent to allow dissolution. The solutions were filtered through a 0.45 μm polytetrafluoroethylene syringe filter and were then injected into a size-exclusion chromatography system equipped with a Jordi xStream GPC column at a flow rate of 0.8 ml/min and analyzed with refractive index and right-angle light scattering detectors.

In Paper V, molar mass was determined using gel permeation chromatography with a 0.5% w/v LiBr/DMSO solvent. The samples were analyzed with three serial columns (Agilent PolarGel 300 × 7.5 mm i.d., Agilent, Germany) equipped with a Kontron

420 high-performance liquid chromatography pump, pulse damper, UltiMate 3000 autosampler, UltiMate 3000 column oven, UltiMate 3000 UV detector (all UltiMate devices from Dionex), and Shodex RI-101 refractive index detector.

3.4 Uronic acid content

Determination of uronic acids was performed using the Blumenkrantz and Asboe-Hansen [78] method. In Paper II, 10 mg of xylan was hydrolyzed with 0.5 ml of cold 96% sulfuric acid, followed by 5 min stirring with vortex and the addition of 0.25 ml of cold water before stirring again for 5 min. This step was performed twice, and the sample was then diluted with water to 10 ml and diluted again with a 9:1 water–sulfuric acid solution because the concentration of the first dilution was over the detection range. Then 160 μl dilute hydrolysate, 20 μl sulfamic acid-potassium sulfamate, and 800 μl sodium tetraborate in sulfuric acid were added to Eppendorf plastic tubes. The solution was heated to 95 °C for 20 min. As a coloring agent, 40 μl of 0.15% w/v 3-phenylphenol, which turns pink when in contact with uronic acids, was added to the solution, cooled down, and analyzed with UV-Vis spectrometer. An intensity at 525 nm, which is a characteristic of the pink color agent, was recorded and translated to a percentage of uronic acid content using a previously made calibration curve.

3.5 Determination of degree of oxidation

The degree of oxidation (DO) was determined using UV spectroscopy (Papers I, II, and V), nuclear magnetic resonance (NMR) spectroscopy (Paper I), and via determination of number of intact monosaccharides (Paper V). Calibration based on absorbances at 290 nm of periodate solutions (0.1–10 mM) was used to track the consumption of periodate during oxidation. Absorbances at 290 nm of each calibrating solution were recorded and absorbance intensity versus concentration was plotted. Xylan in the solution background was recorded prior to oxidation. When the oxidation was initiated, the UV spectrum of the solution was collected once an hour until 6 h and again at 24 h. Xylan background was subtracted from the measured absorbance under the assumption that this background does not change as oxidation proceeded. The DO was then calculated

through the amount of unreacted periodate left in the solution (Equation 6). Note that AXU is an anhydroxylose unit.

$$\%\mathrm{DO} = \frac{\text{mole of periodate consumed}}{\text{mole of AXU}} \times 100 \quad (6)$$

Quantitative ^{13}C NMR spectra of xylan and DalXs were used to estimate DO using Equation 7 through an integral of total area at the intact C3 position.

$$\%\mathrm{DO}_{\mathrm{NMR}} = \frac{\int \mathrm{C3}_{\mathrm{DalX}}}{\int \mathrm{C3}_{\mathrm{xylan}}} \times 100 \quad (7)$$

Also the difference in total xylose content between xylan and modified xylan was translated to DO. Detection was performed as outlined in Section 3.2.

3.6 Hydrodynamic diameter

In Papers I and V, the dynamic light scattering technique was employed using Nanosizer® ZS90 (Malvern Panalytic, UK). Xylans and their derivatives were solubilized in Milli-Q water or phosphate buffer solution (PBS) (pH 7.4) at the target concentration overnight. The solutions were filtered using a 0.45 μm polyvinylidene difluoride filter prior to measurement. The instrument was set to measure three times after 120 s of calibration time. Hydrodynamic diameter (D_h) was calculated with Zetasizer software using the Stokes–Einstein equation (Equation 8). The experiments were performed at 22 °C, and the viscosity of water was used as given by Zetasizer software (0.000954 Pa·s).

$$D_h = \frac{kT}{3\pi\eta D} \quad (8)$$

Where k is Boltzmann's constant, T is absolute temperature, η is viscosity and D is transitional diffusion coefficient.

A similar approach was used to determine the D_h of xylans and modified xylans in Paper II. The D_h in this case was measured in DMSO using Litesizer 500 (Anton Paar, Austria). The xylans and modified xylans were pre-swelled in small amounts of water before being dissolved in DMSO, and the solutions were used without filtering. The

experiments were performed at 25 °C and viscosity of DMSO was 0.00199 Pa·s [79]. Kalliope™ software was used to calculate number distribution and diffusion coefficient.

3.7 Polysaccharides thin film preparation

Three different substrates were used to support the polysaccharide films. Silicon substrates (Siegert Wafers, Germany) were primarily used for validating film forming procedures, morphology study, and thickness analysis. Commercial sensors for QCM-D (Quartz Pro AB, Sweden) and SPR (BioNavis Ltd., Finland) with additional silicon oxide layers were used for various analyses, such as thickness, stability, and adsorption.

The xylan and DalX films in Paper II were prepared by pre-swelling in 30 μl water before dissolving in DMSO (5 mg/ml). The films were coated directly on a QCM-D sensor or silicon substrate using a spin-coater set at 4,000 rpm for 3 min. The chamber was flushed with N_2 to avoid a DMSO saturated environment. Two layers were coated to ensure full coverage of the film.

Xylan was prepared at 5 mg/ml with a similar approach as in Paper II, but 500 μl water was used for 30 ml of solution. Kraft lignin (1,600 g/mol) was dissolved directly in DMSO at the same concentration. Mixtures of lignin–xylan were made at 20:80, 50:50, and 80:20 mass ratios. These solutions and mixtures were spin coated on a silicon wafer at 4,000 rpm for 4 min.

In Paper IV, trimethylsilyl cellulose (TMSC)-hydroxypropyl cellulose stearate (HPCE) blend films were prepared. First, TMSC and HPCE were dissolved separately in chloroform (0.75 wt%) at 30 °C for 120 h, followed by filtering using a 0.45 μm PVDF filter. The spin-coating solution was made by mixing solutions with different TMSC–HPCE ratios: 1:0, 1:3, 3:1, and 0:1. The spin-coating speed was set at 4,000 rpm for 1 min. The films were exposed to HCl vapor to convert TMSC to cellulose.

Cellulose films in Paper V were prepared by dispersing 1.7 g/l CNF or TCNF in water and sonicating and centrifuging the suspension. After that, the supernatant was separated and used for spin coating. A spin-coater was programmed at 3,000 rpm for 1 min. Two layers of cellulose were coated to ensure full coverage.

3.8 Thin film morphology evaluation

Atomic force microscopy (AFM) is a surface-sensitive technique that uses nanoscale (sharp) tip scans line by line across a surface. The detector records the movement of the tip and translates it into a topography image of the scanned area [80]. This gives information on film morphology, such as uniformity and surface roughness. The topography of the films was observed with tapping mode using NTEGRA AFM (NT-MDT, Russia) equipped with Tap300Al-G tips in Paper II and Paper III, and NSG01 tips were used in Paper V. The observation was done in at least three different positions. Collaborators in Paper III and Paper IV performed measurements with Asylum Research MFP-3D AFM (USA) equipped with an Olympus AC160TS tip.

3.9 Evaluation of film thickness

The thickness of Paper II films was determined with AFM. Films on silicon substrates were scratched with a sharp wooden object to ensure the removal of the film without damaging the substrate. A height difference between the film and substrate was determined as film thickness at three positions using the same setting as for the morphology imaging.

The thickness of the thin films was also investigated with QCM-D (Q-Sense E4, Biolin Scientific, Sweden) in Papers II and V. With QCM-D, films were exposed to air at a flow rate of 100 μl/min (Paper V) and 400 μl/min (Paper II). The frequency change was recorded using Qsoft401 software. The data were analyzed using the Sauerbrey equation (Equation 3) followed by thickness (d) estimation through assuming film density (Equation 9). Note that the film density ($\rho_{assumed}$) of the thin film for cellulose in Paper V is 1,500 kg/m^3 and the xylan film in Paper II is 1,200 kg/m^3.

$$d = \frac{m}{\rho_{assumed}} \tag{9}$$

3.10 Humidity response and swelling of the films

In Paper II, xylan and DalX films were exposed to humidity generated by saturated $CaCl_2$, NaCl, and K_2SO_4 salt solutions, which gave 26%, 75% and 97% relative humidity

(RH), respectively, for 1.5 h per RH level. The response was recorded, and the amount of water adsorbed by the films was calculated using Equation 3.

The amount of water incorporated in thin films was determined with H_2O/D_2O solvent exchange performed on QCM-D (Paper V). The difference in the resonance frequency between H_2O and D_2O at the plateau was used according to Equations 10 and 11.

$$\left(\frac{\Delta f}{n}\right)_{\text{water}} = \frac{\left(\frac{\Delta f}{n}\right)_{\text{film}} - \left(\frac{\Delta f}{n}\right)_{\text{bare}}}{\left(\frac{\rho_{D_2O}}{\rho_{H_2O}}\right) - 1} \tag{10}$$

$$\Gamma_{water} = -C\left(\frac{\Delta f}{n}\right)_{water} \tag{11}$$

Where $(\Delta f/n)_{\text{water}}$, $(\Delta f/n)_{\text{film}}$, $(\Delta f/n)_{\text{bare}}$, ρ_{H_2O}, ρ_{D_2O} and C have different frequencies due to water mass, different frequencies between H_2O and D_2O on bare sensor, different frequencies between H_2O and D_2O after film deposition or adsorption, density of H_2O, density of D_2O, and sensitivity constant of quart sensor, respectively.

3.11 Adsorption of xylan derivatives

In Paper V, two surface-sensitive techniques were used to quantify DAX affinity toward cellulose surfaces using QCM-D and SPR. DAXs (1 mg/ml) were dispersed in PBS (100 mM NaCl and pH 7.4). First, the films were pre-swelled in PBS until resonance frequency reached a plateau. Then, the DAX solution was pumped through the chamber for 2 h and rinsed with PBS to remove unbinding molecules. Equations 3 and 4 were used to estimate DAX mass adsorbed on cellulose films. The same procedure was employed with SPR, but at a flowrate of 10 μl/min. Adsorbed masses were calculated using Equation 5. Note that kd_p can be considered a constant at a specific wavelength when the layer is thinner than 100 nm. The value of kd_p is 0.91×10^{-7} cm/° at 670 nm and 1.56×10^{-7} cm/° at 975 nm.

4
RESULT AND DISCUSSION

4.1 Xylan derivatives via periodate oxidation

The properties of extracted wood xylans are influenced by their composition and structure. Backbone chain length, branching, and the number of monosaccharides and uronic acid substituents contribute to solubility [24, 30, 31, 34]. Four xylans were selected, and their composition and molar mass were determined to enable a comparison of their characteristics in a solution (Table 1). Their dry appearances varied from fine powder to small granules and flake-like shapes with a yellow tint. Their composition varied from 96 wt% to 99 wt% xylose, with a small amount of other monosaccharides (< 1 wt% to almost 5 wt%) and uronic acids. The molar mass of the xylans varied from 7,700 to 31,000 g/mol.

Table 1. Carbohydrate composition, uronic acid content, and molar mass of unmodified xylans

Paper	**Wood species**	**Relative carbohydrate composition (wt%)**				**Uronic acid (mol%)**	**Molar mass (g/mol)**
		Xylose	**Glucose**	**Galactose**	**Arabinose**		
I and III	Beech	96	< 2	< 2	< 1	12	23,800
II and III	Beech	99	0	0	0	8	14,000
V, LX	Beech	98	2	0	< 1	8	7,700
V, HX	Birch	98	1	0	< 1	7	31,000

Xylans were modified using sodium periodate, which alters their structure to an oxidized form called dialdehyde xylan. In some grades, they were further reduced to a more stable form using sodium borohydride, which is called dialcohol xylan. The UV spectroscopy method was used to determine DO based on the amount of unreacted periodate in the solution. Maekawa et al. [81] used this method to quantify the DO of periodate oxidized cellulose. In general, for this quantification, the solution was filtered to remove the components other than the periodate before the filtrate was examined with UV spectroscopy. However, xylan, which was partially dissolved in water, could not be completely removed from the solution by filtering, in the same way as is possible, for example, for cellulose fibers, despite using a small-pore size filter (0.2 μm). Small xylan aggregates that passed through the filter may have caused light scattering, which interfered with the analysis [82], while the oxidized product, DAX, was expected to be more soluble due to the opening of the monosaccharide ring at the backbone [83]. Consequently, the analysis was performed without a filtering step, and xylan background was instead subtracted from the spectra. Nevertheless, a mixture of xylan and DAX at different ratios over the oxidation had a spectrum that differed from the initial xylan used as background (Figure 10). Specifically, the spectrum corresponding to xylan dispersed in water showed higher absorbance than DAX at 290 nm.

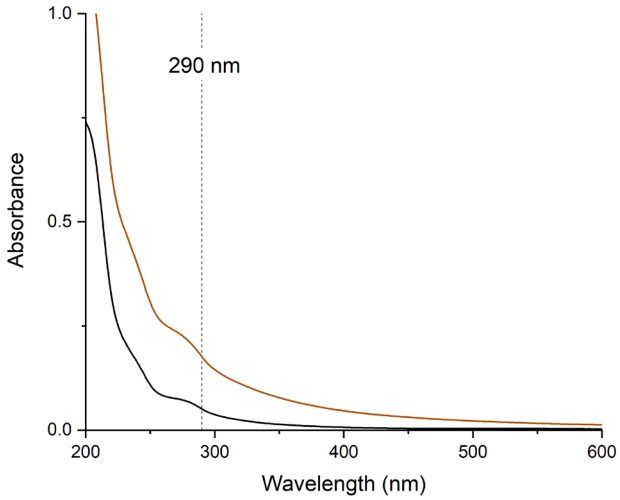

Figure 10. UV-Vis spectrum of xylan (brown) and dialcohol xylan (black) in water. Originally published in Palasingh et al. [84], and licensed under CC BY 4.0

Even though UV spectroscopy is a quick and simple method to determine DO, due to the tendency to overestimate DO [82], there is a benefit to complementing it with other

analytical techniques, such as infrared spectroscopy [85], NMR spectroscopy [86], and titration [87, 88]. NMR spectroscopy was used for DO determination in Paper I and found that the DO value was lower than what was found using UV spectroscopy by about 4–7% (Table 2). In Paper V, carbohydrate composition was used as an indirect method to complement the DO analysis by comparing the number of monosaccharides detected before and after the modification of xylan. The DO was estimated to be 92% and 94% for high molar mass DAX (HX) and low molar mass DAX (LX), respectively, which is close to values determined using UV spectroscopy (92% for both grades).

Table 2. Degree of oxidation and molar mass of xylan derivatives

Paper and Sample	Xylan derivative	DO (%)		Molar mass (g/mol)
		UV	Other method	
I, DalX1	DalX	84	77[a]	18,700
I, DalX2		84	80[a]	18,200
I, DalX3		84	77[a]	18,300
I, DalX4		84	79[a]	18,000
II, DalX80	DalX	77	n. a.	10,500
II, DalX60		63	n. a.	12,200
II, DalX40		42	n. a.	14,500
V, LX	DAX	92	94[b]	5,100
V, HX		92	92[b]	13,000

a – Determined using NMR spectroscopy
b – Determined using carbohydrate compositional analysis

The effect of quenching the unreacted periodate and removing species other than DAX before borohydride reduction on the properties of the product was investigated using different pathways (Figure 11, path i–iii). The first path (i) was the fastest, wherein borohydride solution was added right after the oxidation time reached 24 h. Excess IO_4^-

and byproduct IO_3^- presented in the solution together with DAX. Borohydride could be consumed by both IO_4^- [89] and IO_3^-, which may lead to a risk of partial reduction because both ions may devour the majority of reductants due to their concentration. Quenching with ethylene glycol was performed before the reduction in the second path (ii). Although ethylene glycol removed IO_4^-, the remaining ethylene glycol may consume borohydride, which led to a similar problem as in the first path. In the third path, purification was carried out. On comparing DalX from these three paths, they were found to be quite similar in molar mass (Table 2).

Borohydride reduction was anticipated to reduce molar mass during the reaction, a countermeasure using NaH_2PO_4 with a shorter reaction time was employed to maintain pH and minimize degradation (path (iv)) [90]. DAX was fully reduced within 4 h. The molar mass of DalX from paths (iii) and (iv) were fairly similar. NaH_2PO_4 did not show a significant difference except that dispersity was higher (M_w/M_n 2.2) compared to mere borohydride reduction in the third path (M_w/M_n 1.9).

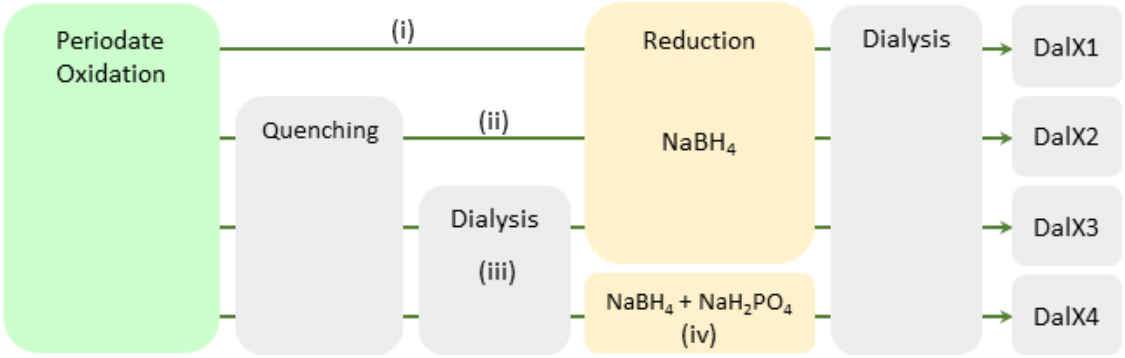

Figure 11. Periodate oxidation and borohydride reduction sequences. Originally published in Palasingh et al. [84], and licensed under CC BY 4.0

Periodate oxidation of xylans showed an unavoidable degradation of the xylan chain, indicated by the decreasing molar mass (Table 1 and Table 2), even though having a radical scavenger and performing the reaction shielded from light were used as countermeasures to prevent degradation. Periodate concentration has been found to directly relate to molecular degradation through glycosidic bond cleavage, and, consequently, a peeling reaction occurs at newly generated reducing end groups [44, 91]. Not only molar mass reduction was affected by periodate concentration, but also yield was found to be lower at higher periodate concentration. A yield of DalXs was 70%, 49%,

and 30% for 1:0.4, 1:0.6 and 1:1 AXU–periodate mole ratio, respectively. At the same 1:1 ratio, a longer reaction time (96 h) in Paper V led to higher DO; however, it caused a more severe decrease of the molar mass in comparison to the shorter oxidation time (24 h) used in Paper I. Especially with HX (Paper V), the chain length reduced by more than half.

The oxidation kinetics were faster at high periodate concentration, as a larger reaction constant (0.82 s^{-1}) was found at 1:1 AXU to periodate moles ratio than 1:0.6 and 1:0.4 ratio, where the reaction constant was 0.45 s^{-1} in both cases (Figure 12). Regardless of the AXU to periodate mole ratio, most periodate was consumed during the first 6 h.

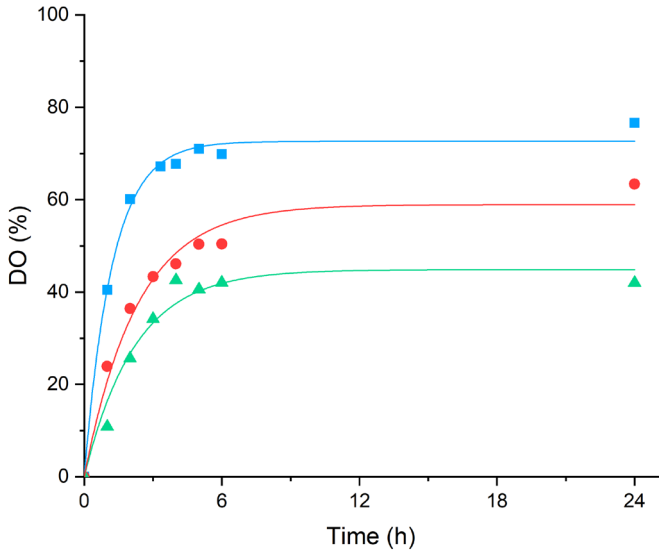

Figure 12. Oxidation progress of beechwood xylan using AXU to periodate moles ratio 1:1 (blue), 1:0.6 (red), and 1:0.4 (green). The reaction was fitted with a first-order kinetic model. Reproduced from Paper II manuscript

4.2 Solubilization of xylans and their derivatives

Regardless of the xylan composition and molar mass (Table 1), water-based xylan mixtures were turbid and pale yellow or brownish solutions, where these appearances were the result of microscale xylan aggregates (Figure 13). The beechwood xylan with a higher number of substituents (Paper I) was visually better dispersed (in water) than the beechwood xylan (Paper II) that had lower molar mass with a low number of substitutions. This is evidence of the influence of the substituents in interrupting the close packing of xylan chains [30]. Other means to increase solubilization were considered, such

as ethanol–water cosolvent, sonication, heating, and dissolution in alkaline media. Sonication and alkaline solution were expected to dissolve xylan up to a certain concentration, but degradation was anticipated as well [34]. DMSO is an organic solvent that has the ability to dissolve a wide range of substances and is miscible with water [92]. Xylans could not be directly dissolved in DMSO, and the xylan structure had to be swollen with water prior to incorporating DMSO. This visually improved xylan solubilization (transparent solution) up to a specific concentration, which is in agreement with the findings of Ebringerova et al. [34], who reported that water-insoluble arabinoxylan in a 9:1 volume fraction of DMSO to water was more efficiently solubilized than in DMSO. However, high molar mass xylan, such as 31,000 g/mol, did not solubilize in DMSO/water.

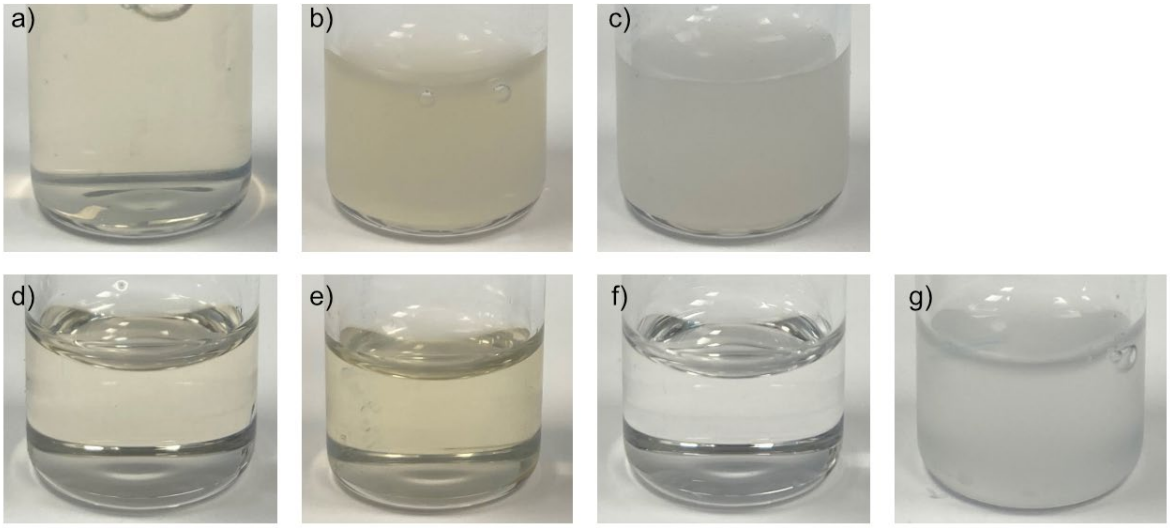

Figure 13. Xylans dissolved in water (top row) and DMSO (bottom row) at 10 mg/ml of a,d) beechwood xylan 24,000 g/mol, b,e) beechwood xylan 14,000 g/mol, c,f) beechwood xylan 7,700 g/mol, and g) birchwood xylan 31,000 g/mol

The D_h of xylans and their derivatives was explored as a representation of their solubilization through evaluation of the size of the clusters in a specific solvent. DalXs in Paper I were water soluble and showed a similar D_h in water to unmodified xylan at concentrations ≤ 0.5 wt% (Figure 14). At this concentration, xylan and DalX had similar D_h, with a 21–26 nm range. The D_h of xylan increased to 52 nm at 2 wt%, while the D_h of DalXs remained at a similar level (< 30 nm), even when dispersed at 2 wt%, except when prepared via an oxidation route where the reduction was done directly after oxidation (black data points in Figure 14). Modified xylan prepared in this way had a D_h of 32 nm at

2 wt%, which is still smaller than the 52 nm large cluster of the non-modified xylan. Note that the D_h of xylan does not represent the entire population of the solution, since it was filtered prior to analysis and aggregates larger than 0.45 μm were removed.

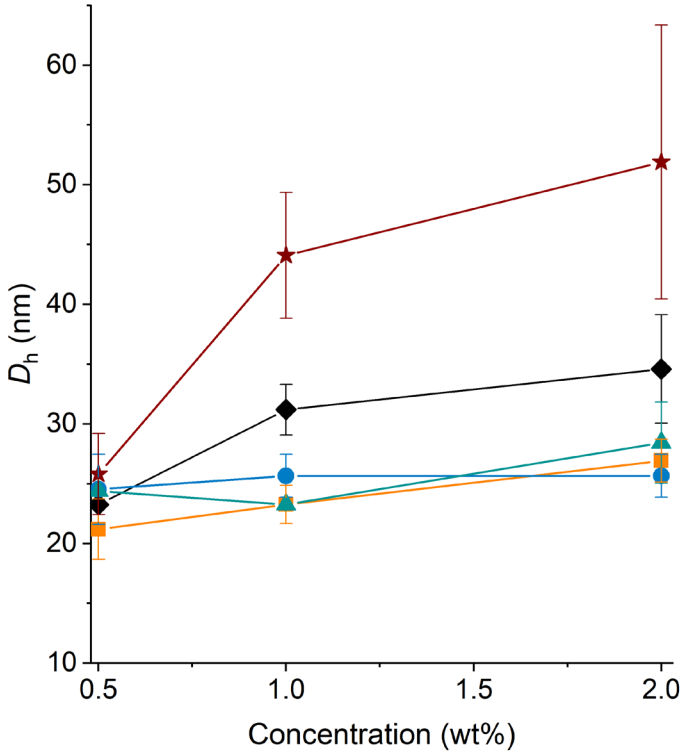

Figure 14. Hydrodynamic diameter by number distribution of xylan (★), DalX1 (◆), DalX2 (■), DalX3 (●), and DalX4 (▲) dissolved in water. Originally published in Palasingh et al. [84], and licensed under CC BY 4.0

The xylan derivative DalXs (Paper II), which were prepared using xylan with 14,000 g/mol molar mass and 8% of uronic acids. This implies that the modification that opened the monosaccharide ring was not enough to fully solubilize them in water, but that the properties of the starting xylan have a decisive effect on the properties of the derivative. Visually, 77% DO (DalX80) performed better than other, lower DOs in dissolution, but it still resulted in a turbid solution (Figure S1 Supporting Information Paper II). Visually, xylan and DalXs fully dispersed in DMSO. Surprisingly, however, only DalX80 showed an obvious decrease in D_h, from 205 nm to 60 nm after modification at 5 mg/ml (Figure 15). This suggests that a higher DO is required for solubilization of unbranched chain xylan than for branched xylan. The modification also narrowed the size distribution.

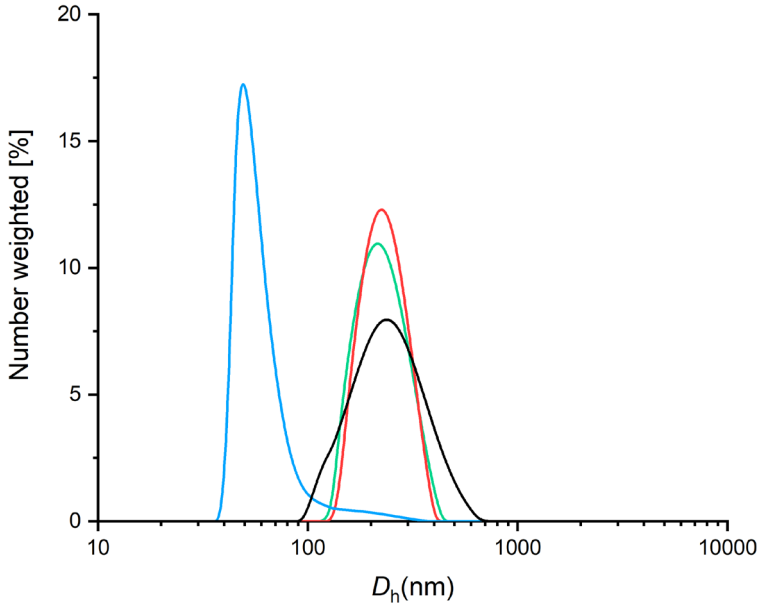

Figure 15. Number distribution of hydrodynamic diameter of dissolved xylan derivatives in DMSO (5 mg/ml). Xylan (black), DalX40 (green), DalX60 (red), DalX80 (blue). Reproduced from Paper II manuscript

4.2 Stability of xylans and their derivative films

Xylans were made into films, and several approaches involving different solvents were employed with the goal of achieving a closed film. Alkaline solution, for instance 0.5 M or higher sodium hydroxide, can dissolve xylan (5 mg/ml), but it was expected to leave residual salts in the dry film. Even though these granules were easily removed through neutralization with acid, such as hydrochloric acid, holes where the granules sat could be seen with AFM (results not shown here). Using DMSO/water as the solvent, the low vapor pressure of DMSO necessitated the use of a high rotation speed, long coating time, and flushing the chamber with air or N_2 to allow the solvent to completely evaporate. At a concentration of 5 mg/ml (Paper II) with two layers deposited, closed xylan films were unfortunately not obtained, but instead, uniform discontinuous clusters were observed (Figure 16a). The influence of DO on thin film formation was investigated with the derivatives of this xylan grade. An increase in DO increased the size of the xylan clusters and resulted in lower surface coverage of DalX40 and DalX60 compared to the unmodified xylan film (Figure 16b–c). When DO reached 77%, DalX did not form clusters, and smooth films were obtained (Figure 16d).

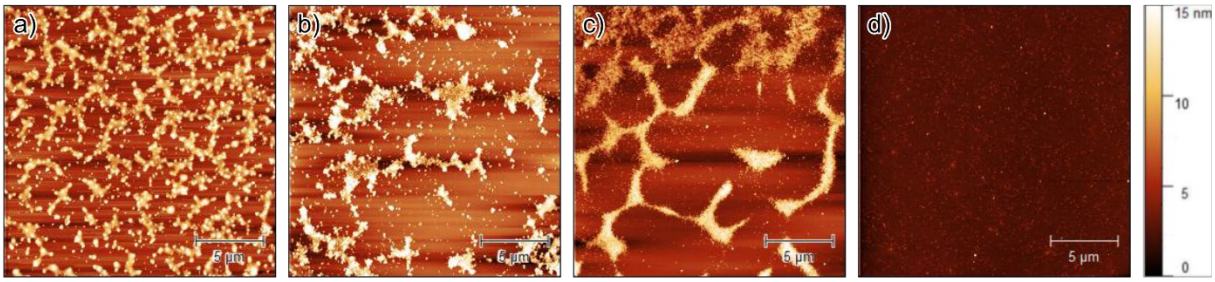

Figure 16. AFM topography (a) xylan film; (b) DalX film at 42% DO (c) DalX film at 63% DO (d) DalX film at 77% DO. Reproduced from Paper II manuscript

The xylan and DalX films were exposed to humid air. The DaIX60 films were not studied because their behavior was expected to be similar to that of DaIX40 based on their morphological resemblance (Figure 16b–c). It was assumed that due to the hydrophilicity of xylan and its derivatives, the higher the RH, the more water retained in the films. This was found to be true for the xylan and DaIX films (Figure 17a-c). Interestingly, water vapor adsorbed by the film was independent of the film mass for xylan (Figure 17a) and DalX40 (Figure 17b). Note that the value for the amount of water in the film may be obscured since the films of xylan and DalX40 were not closed films. Especially for DalX40, the difference between each RH level was smaller than for xylan films, which may be due to the larger uncovered surface. On the other hand, in DalX80 films, the amount of water had a tendency to increase with increasing film mass (Figure 17c).

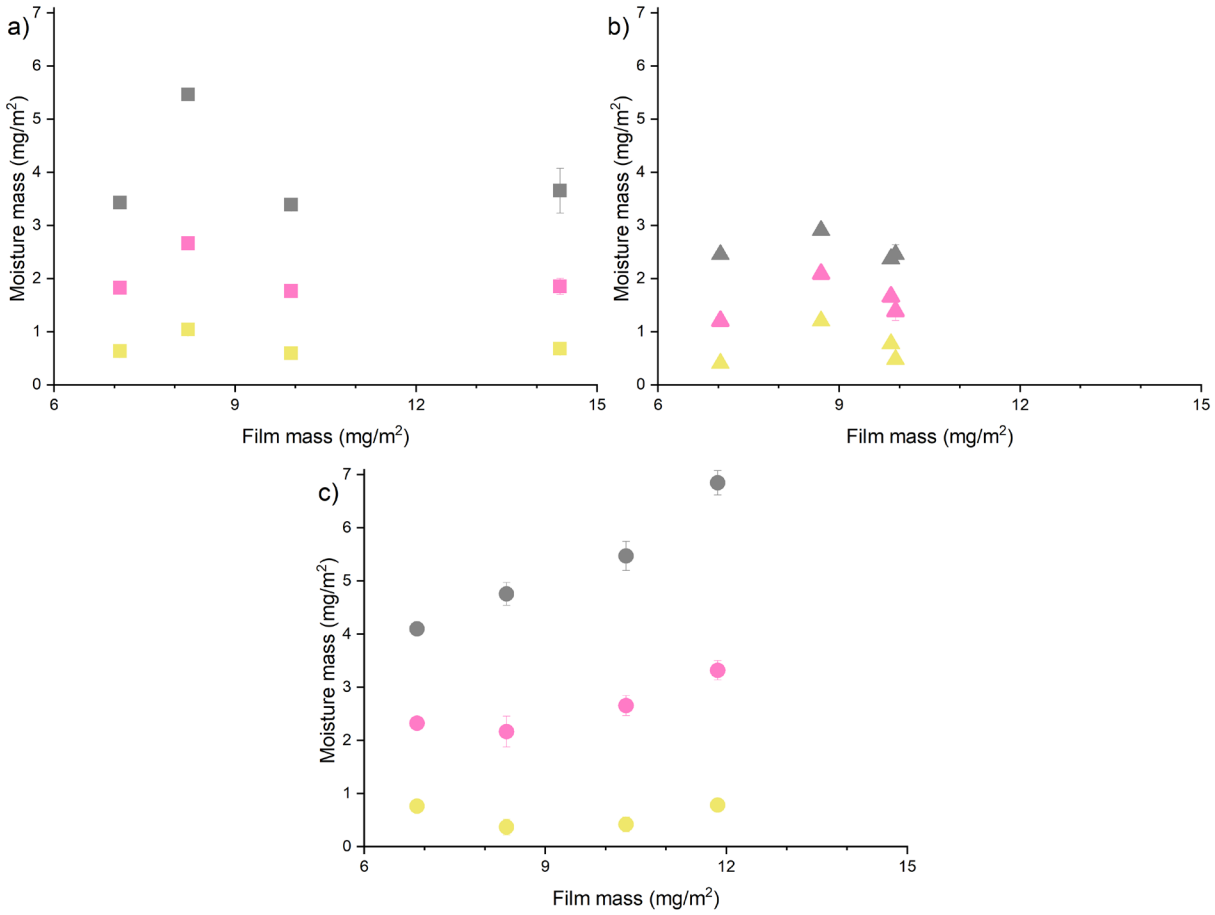

Figure 17. Adsorbed amount of water vapor on (a) xylan (b) DalX40 (c) DalX80 after exposure to 26% RH (yellow), 75% RH (pink), 97% RH (gray). Reproduced from Paper II manuscript

Water incorporated into the films was expected to increase the dissipation value. However, the films were quite thin (less than 15 nm); hence, the response was expected to be small. When comparing xylan to DalX80 films (Figure 18), there was no significant difference between them at 26% RH and a slight difference at 75% RH. At 97% RH, the dissipation of DalX80 rapidly increased from 0.5×10^{-6} to almost 2×10^{-6} when 4–7 mg/m^2 of water was adsorbed into the film. Arabinoglucuronoxylan self-standing films have shown a faster response to RH levels than observed here, which is likely due to intrinsic hydrophilicity of arabinose and glucuronic acid side groups [93].

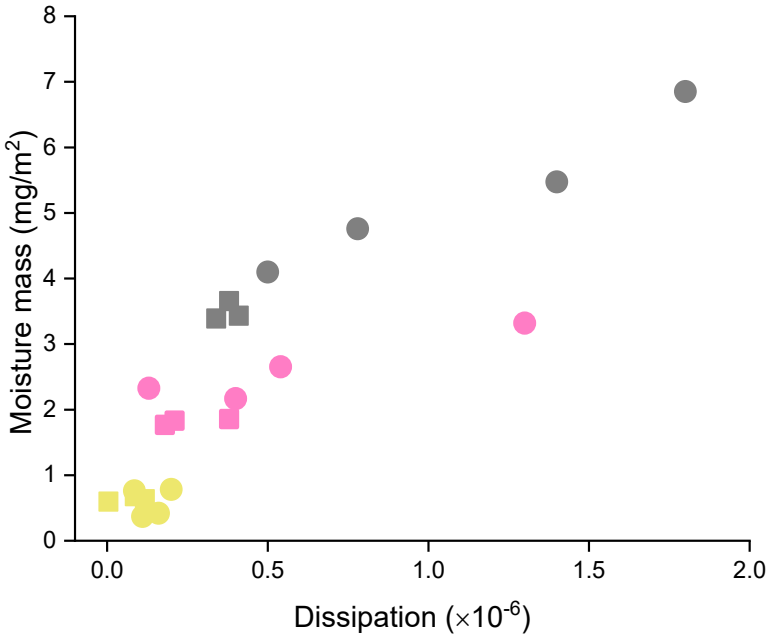

Figure 18. Mass of adsorbed moisture against dissipation of xylan (square) and DalX80 (circle) after exposure to 26% RH (yellow), 75% RH (pink), 97% RH (gray). Reproduced from Paper II manuscript

4.3 Polysaccharides in blend films

Tuning of film properties such as friction, morphology, or wetting properties may be required for their use. In this thesis, morphology was diversified using blend solutions to make films and pattern the films via phase separation of the blend components as the film was formed during solvent evaporation.

Biphasic film from cellulose derivatives formed spinodal decomposition patterns at various TMSC–HPCE volume ratios and modified the film surface morphology in Paper IV (Figure 19a). HPCE created cavities at 75:25, while TMSC formed tall spikes at 25:75. After films were exposed to HCl vapor, silyl groups were cleaved, and the film thickness decreased, altering the film morphology (Figure 19b): HPCE cavities turned into hills and TMSC spikes developed into cellulose holes for the 75:25 and 25:75 film, respectively. This also revealed that HPCE was a continuous phase in the 75:25 and 50:50 films. At the same time, cellulose, which has different wetting properties from TMSC, influenced the surface wetting and friction of the blend films (Paper IV).

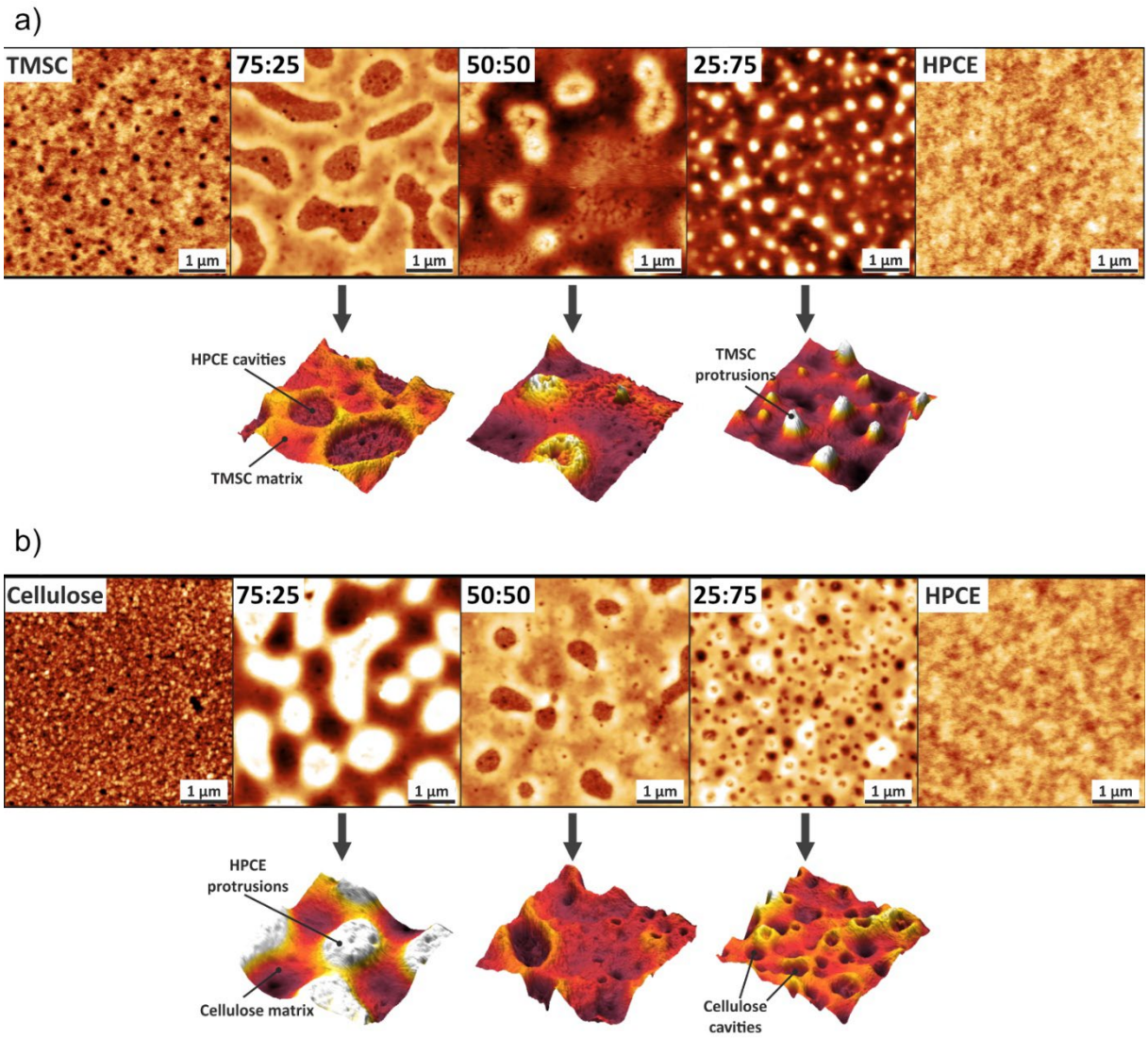

Figure 19. Topography of films at different volume ratios of (a) TMSC–HPCE and (b) cellulose–HPCE. The height scale of neat TMSC, cellulose, and HPCE films was 10 nm, and of blended films 60 nm. Originally published in Czibula et al. [94], and licensed under CC BY 4.0

When it comes to wood-based macromolecules without modification, their low solubility is a challenge for controlling biphasic phase separation in films. In this thesis, DMSO was selected as a solvent to incorporate xylan (14,000 g/mol) and lignin (1,600 g/mol) into blended films (Paper III). Xylan, which was the same grade as was used previously (Paper II), formed fractal patterns (Figure 20a). The difference in the xylan film morphologies (Figures 16a and 20a) may arise from a difference in the water content in the spin-coating solution. Increased xylan–lignin mass ratio from neat xylan to 80:20 and 50:50 resulted in spinodal decomposition patterns; discontinuous clusters with size

of the discontinuous phase decreasing with increase in the lignin fraction (Figure 20b–c). Rounded clusters were formed in 20:80 film (Figure 20d) and were assigned to spinodal decomposition because of the uniform size of the clusters. Lignin (molar mass 1,600 g/mol) formed a continuous film that was expected from fully dissolved lignin (Figure 20e).

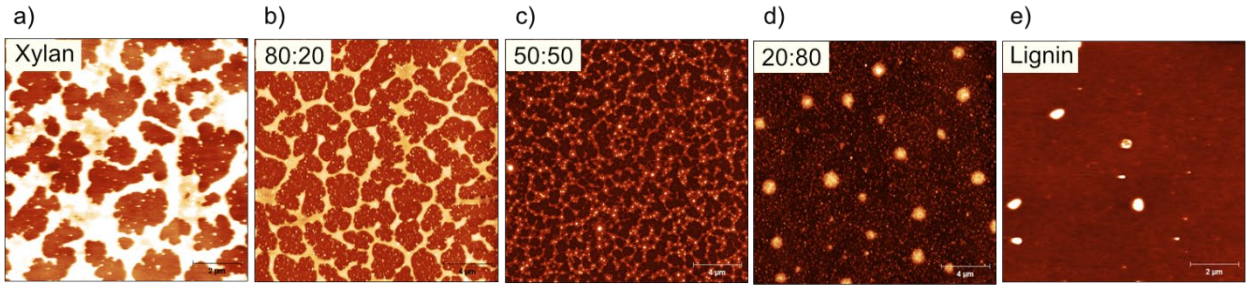

Figure 20. Topography of xylan–lignin blend films at different mass ratios. The blends contained 14,000 g/mol xylan and 1,600 g/mol lignin. The height scale of neat xylan and lignin was 5 nm, and of blended films 20 nm. Reproduced from Paper III manuscript

4.4 Adsorption of modified xylan on cellulose films

Modified xylans in the form of DAXs (Paper V) were explored as film additives for cellulose-based films. CNF and TCNF thin films were prepared using the spin-coating technique. A repulsion of negatively charged TCNF fibrils resulted in thinner films (dry state) compared to CNF films (Figure 21a). In the case of adsorption of DAX on CNF films with a close-to-neutral surface charge, the DAX molar mass was decisive for the adsorbed mass. HX DAX molecules (13,000 g/mol) adsorbed in a higher mass on the close-to-neutral surface (Figure 21b). This may be because the large DAX molecules can form more and larger loops on the surface, which results in a larger adsorbed mass compared to LX DAX (5,070 g/mol). However, this factor was overpowered by the effect of the negative charge of the TCNF films where there is a competition for space between DAX and the counter ions to maintain surface electroneutrality.

DAX, which was adsorbed on the films, reduced swelling of the films by repelling water from the TCNF film surface or network regardless of the molar mass. The opposite effect was found with the CNF films, and their water content increased slightly when DAX was adsorbed. This was confirmed by considering the difference between the QCM-D and

SPR adsorbed masses (Figure 21b). Film thickness in the dry state after DAX adsorption slightly increased on both films (< 2 nm), but the change in LX DAX was statistically insignificant (Figure 21a).

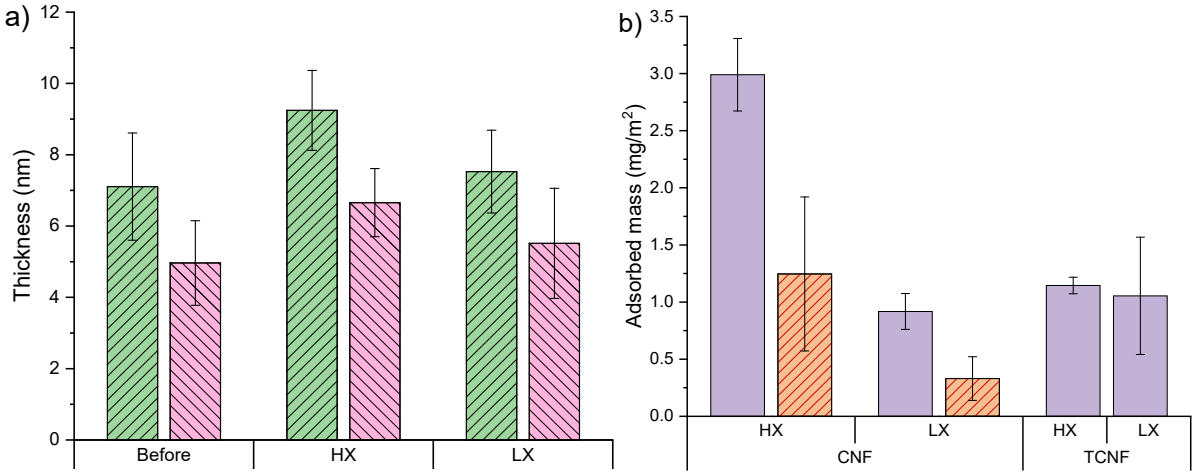

Figure 21. (a) CNF film (green) and TCNF film (pink) thickness determined in dry conditions. (b) Adsorbed mass of DAX on neutral CNF surface (purple) and negatively charged TCNF surface (orange). Originally published in Palasingh et al. [95], and licensed under CC BY 4.0

In the swollen state, the hydration level of DAX-modified CNF films was similar, independent of the DAX molar mass. (Figure 22). In the case of the TCNF films, DAX, regardless of molar mass, decreased the hydration level by at least 10%. DAX led to less water associated in the TCNF films.

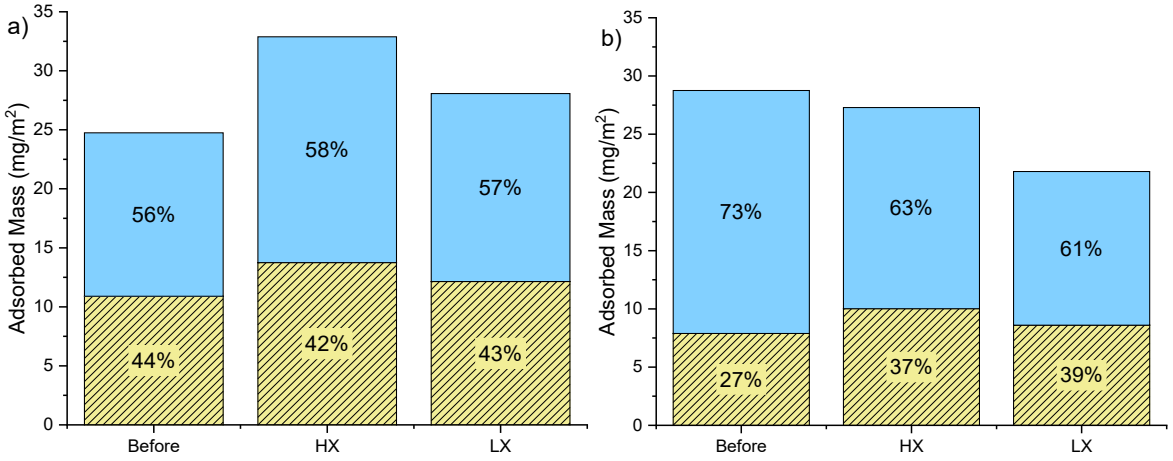

Figure 22. Water coupling on the swollen state of (a) CNF film and (b) TCNF film (right). Originally published in Palasingh et al. [95], and licensed under CC BY 4.0

5
CONCLUSIONS

The properties of wood-based materials can be tuned by chemical and physical modifications. Utilizing xylans from solutions, and hence elucidating on their solubility and water interactions was a primary objective of this thesis research.

Solubilization of xylans depended greatly on their composition, and molar mass. Substitution of xylan backbone seemed to be more decisive than molar mass, which was concluded from observations that 14,000 g/mol xylan with a low number of substituents (< 1% and 8% carbohydrate side groups and uronic acids, respectively) dissolved less well in water and DMSO than 24,000 g/mol xylan higher number of substituents (< 5% carbohydrates and 12% uronic acid substituents). Pre-swelling with water is crucial to solubilize xylan in DMSO, but there is a limit to how high the molar mass of xylan can be.

Periodate oxidation has been suggested to improve flexibility of polysaccharides through backbone ring opening. DAX contains very active aldehyde groups which was further reduced to DalX. A systematic study of performing quenching, and purification before the reduction showed no significant difference in molar mass irrespective of those two steps were done or not, as long as enough reducing agent ($NaBH_4$) was present in the solution to fully reduce DAX. A combination of buffer salt and shortening reaction time in reduction was not obvious to prevent degradation, but 4 h was enough to completely convert DAX to DalX. The results presented here enable a simplified and shortened protocol for reduction of DAX to DalX.

Backbone ring opening via periodate oxidation promoted solubilization, as evidenced by visual observation of the solutions, D_h, and morphology of thin film. DAX and DalX showed less turbid to transparent dispersions than unmodified xylans. DAXs and DalXs became water-soluble up to certain concentration except DalXs produced from

14,000 g/mol xylan. Those DalXs did not fully solubilized in DMSO as well, but there was significant improvement as evident by smaller D_h at equally high DO. The results show that oxidation and reduction of xylan enable solubilization in polar solvents, however, the degree of oxidation required to obtain such effect, depends on initial composition of xylan and thus source.

Xylan derivatives via periodate oxidation were demonstrated in films and as film additives. Xylan thin films showed diverse and inhomogeneous film morphologies, likely related to its poor solubilization prior to spin coating. In contrast, films produced from the derivatives, *i.e.,* DalX80, showed better film formation in terms of homogeneity and reproducibility using spin coating. The films were also more hygroscopic than films from the starting xylan. Incorporation of DAXs in cellulose film as additives showed reduced water content in TCNF films. This benefits for tuning water sensitivity of cellulosic materials.

Xylan, which is often used as an energy source or degraded to monosaccharides and converted to chemicals, such as furfural and xylitol, has tremendous potential in its polymeric form. Periodate modification was demonstrated to improve xylan-solvent interaction. Increasing solubilization through modification produced a beneficial outcome for preparing films. These findings are likely to be applicable for engineering of gels, composites, and coating as well, that may have, e.g., pharmaceutical and medical use.

6
ACKNOWLEDGMENTS

I would like to thank the Swedish Research Council (grant registration number 2017-05138) the SNS Nordic Forest Research (grant number SNS-127) and Vinnova (grant number 2019-03607) for funding my research. Erasmus+ is acknowledged for research visit funding. Chalmersska forskningsfonden and Bo Rydin Foundation are thanked for funding travel grants.

My supervisor Tiina Nypelö and co-supervisor Anna Ström—Thank you for supporting and accompanying me throughout my PhD journey. Encouraging me to do what seemed to be impossible at the beginning afforded me the opportunity to earn my doctorate with your guidance and assistance.

Thank you to Hanna Härelind for being my wonderful examiner.

To all past and present colleagues in the Larsson/Ström/Nypelö groups: Vishnu, Robin, Rydvikha, Roujin, Saul, Mina, Aline, Jakob, Panos, Leo, Ehsan, Pegah, Eliott, Åke, Bahiru, Marina, Donghyun, and Giovanni—We are sharing a lot of life and work experience.

Lotta Pettersson, Frida Andersson, Carina Jogevik, and Anna Oskarsson, our brilliant administrative team—Thank you for your helping and answering questions over these past years.

Thank you to Rupert Kargl and Karin Kleinschek at the Institute IBioSys, TU-Graz for hosting me during my research visit. Thanks also to Stefan Spirk, Florian, Tobias, Urban, Jana, Ivan, Mohan, and Claudia for the many amazing experiences in Austria during my time there.

Thank you, Felix Abik, for helping with SEC, Parveen Kumar Deralia and Kenneth Gacutno Arandia for helping out with HPLC and the Forest engineers for access to the equipment, and Jana Schaubeder for helping with the DLS. And to Koyuru Nakayama, who is an NMR expert and Swedish NMR Centre at the University of Gothenburg for its support. Also, Anette Larsson for wonderful discussion regarding UV-Vis spectroscopy and Jakob Karlsson for helping with uronic acid determination. My research wouldn't have been possible without your cooperation and collaboration. To my other coauthors: Caterina Czibula, Gundula Teichert, Maximilian Nau, Mathias Hobisch, Markus Biesalski, Christian Teichert, Kirsi S. Mikkonen, Panagiotis Spiliopoulos, Hassan Amer, and Lars Evenäs—I deeply appreciate your valuable comments and suggestions. The Chalmers Material Analysis Laboratory (CMAL) is acknowledged for providing access to SPR.

Without support from my family, I wouldn't be who I am or where I am today. Thank you for supporting me in all chapters of my life.

My journey wouldn't be possible without you all; sincerely, thank you!

7
REFERENCES

1. United Nations Department of Economic and Social Affairs, *The global forest goals report 2021*, in *United Nations forum on forests secretariat* 2021.

2. Ahankari, S.S., et al., *Nanocellulose in food packaging: A review.* Carbohydrate Polymers, 2021. **255**: p. 117479.

3. Yadav, M. and F.-C. Chiu, *Cellulose nanocrystals reinforced κ-carrageenan based UV resistant transparent bionanocomposite films for sustainable packaging applications.* Carbohydrate Polymers, 2019. **211**: p. 181-194.

4. Awan, F., et al., *Cellulose nanocrystal–ZnO nanohybrids for controlling photocatalytic activity and UV protection in cosmetic formulation.* ACS Omega, 2018. **3**(10): p. 12403-12411.

5. Guo, Y., et al., *Functional mesoporous silica nanoparticles for delivering nimesulide with chiral recognition performance.* Microporous and Mesoporous Materials, 2020. **294**: p. 109862.

6. Petersen, N. and P. Gatenholm, *Bacterial cellulose-based materials and medical devices: current state and perspectives.* Applied Microbiology and Biotechnology, 2011. **91**(5): p. 1277-1286.

7. Kocić, A., et al., *UV protection afforded by textile fabrics made of natural and regenerated cellulose fibres.* Journal of Cleaner Production, 2019. **228**: p. 1229-1237.

8. Poveda-Giraldo, J.A., J.C. Solarte-Toro, and C.A. Cardona Alzate, *The potential use of lignin as a platform product in biorefineries: A review.* Renewable and Sustainable Energy Reviews, 2021. **138**: p. 110688.

9. Heinze, T., et al., *Polysaccharides I: Structure, characterization and use*. 2005: Springer.

10. Miletzky, A., et al., *Modifying cellulose fibers by adsorption/precipitation of xylan.* Cellulose, 2015. **22**(1): p. 189-201.

11. Henriksson, Å. and P. Gatenholm, *Controlled assembly of glucuronoxylans onto cellulose fibres.* Holzforschung, 2001. **55**(5): p. 494-502.

12. Prakobna, K., et al., *Strong reinforcing effects from galactoglucomannan hemicellulose on mechanical behavior of wet cellulose nanofiber gels.* Journal of Materials Science, 2015. **50**(22): p. 7413-7423.

13. Dalvi, L.C., et al., *Study of xylan and cellulose interactions monitored with solid-state NMR and QCM-D. Holzforschung*, 2020. **74**(7): p. 643-653.

14. Köhnke, T., et al., *The effect of barley husk arabinoxylan adsorption on the properties of cellulose fibres.* Cellulose, 2008. **15**(4): p. 537-546.

15. Kabel, M.A., et al., *Structural differences of xylans affect their interaction with cellulose.* Carbohydrate Polymers, 2007. **69**(1): p. 94-105.

16. Amer, H., et al., *Synthesis and characterization of periodate-oxidized polysaccharides: dialdehyde xylan (DAX).* Biomacromolecules, 2016. **17**(9): p. 2972-2980.

17. Ek, M., G. Gellerstedt, and G. Henriksson, *Wood chemistry and wood biotechnology*. 2009, Germany: De Gruyter, Inc.

18. Sixta, H., *Handbook of pulp*. 2006: Wiley-vch.

19. Haygreen, J.G. and J. Bowyer, *Forest product and wood science.* Lowa State University press, 1982.

20. Gibson, L.J., *The hierarchical structure and mechanics of plant materials.* Journal of the royal society interface, 2012. **9**(76): p. 2749-2766.

21. Koch, G., *Raw material for pulp*, in *Handbook of Pulp*. 2006, Wiley-Vch. p. 21-68.

22. Gatenholm, P. and M. Tenkanen, *Hemicelluloses: science and technology*. 2003, Washington, DC, United States: American Chemical Society.

23. Teleman, A., *Hemicelluloses and Pectins*, in *Pulp and paper chemistry and technology - wood chemistry and biotechnology, Volume 1*, M. Ek, G. Gellerstedt, and G. Henriksson, Editors. 2009, De Gruyter: Berlin/Boston, Germany.

24. Ebringerová, A. and T. Heinze, *Xylan and xylan derivatives–biopolymers with valuable properties, 1. Naturally occurring xylans structures, isolation procedures and properties.* Macromolecular rapid communications, 2000. **21**(9): p. 542-556.

25. Pawar, P.M.-A., et al., *Acetylation of woody lignocellulose: significance and regulation.* Frontiers in plant science, 2013. **4**: p. 118-118.

26. Cowie, J.M.G. and V. Arrighi, *Polymers: chemistry and physics of modern materials*. 2007: CRC press.

27. Carraher Jr, C.E., *Introduction to polymer chemistry*. 2017: CRC press.

28. Laine, C., et al., *Hydroxyalkylated xylans–Their synthesis and application in coatings for packaging and paper.* Industrial crops and products, 2013. **44**: p. 692-704.

29. Kishani, S., et al., *Influence of solubility on the adsorption of different xyloglucan fractions at cellulosewater interfaces.* Biomacromolecules, 2019.

30. Guo, M.Q., et al., *Polysaccharides: structure and solubility.* Solubility of polysaccharides, 2017. **2**: p. 8-21.

31. Bosmans, T.J., et al., *Assembly of debranched xylan from solution and on nanocellulosic surfaces.* Biomacromolecules, 2014. **15**(3): p. 924-930.

32. Gröndahl, M., A. Teleman, and P. Gatenholm, *Effect of acetylation on the material properties of glucuronoxylan from aspen wood.* Carbohydrate Polymers, 2003. **52**(4): p. 359-366.

33. Whistler, R.L., *Solubility of polysaccharides and their behavior in solution*, in *Carbohydrates in Solution*. 1973, American Chemical Society p. 242-255.

34. Ebringerova, A., et al., *Solution properties of water-insoluble rye-bran arabinoxylan.* Carbohydrate Polymers, 1994. **24**(3): p. 161-169.

35. Malaprade, L., *Oxidation of some polyalcohols by periodic acid—applications.* Comptes Rendus, 1928. **186**: p. 382-384.

36. Bobbitt, J., *Periodate oxidation of carbohydrates*. Advances in carbohydrate chemistry. Vol. 11. 1956: Elsevier. 1-41.

37. Zeronian, S., F. Hudson, and R. Peters, *The mechanical properties of paper made from periodate oxycellulose pulp and from the same pulp after reduction with borohydride.* Tappi, 1964. **47**: p. 557-564.

38. Sirviö, J., et al., *Synthesis of highly cationic water-soluble cellulose derivative and its potential as novel biopolymeric flocculation agent.* Carbohydrate Polymers, 2011. **86**(1): p. 266-270.

39. Dash, R., T. Elder, and A.J. Ragauskas, *Grafting of model primary amine compounds to cellulose nanowhiskers through periodate oxidation.* Cellulose, 2012. **19**(6): p. 2069-2079.

40. Dacrory, S., et al., *Innovative synthesis of modified cellulose derivative as a uranium adsorbent from carbonate solutions of radioactive deposits.* Cellulose, 2020. **27**(12): p. 7093-7108.

41. Amer, H., et al., *Synthesis and characterization of periodate-oxidized polysaccharides: dialdehyde xylan (DAX).* Biomacromolecules, 2016. **17**(9): p. 2972-80.

42. Sulaeva, I., et al., *Determination of molar mass distributions of highly oxidized dialdehyde cellulose by size exclusion chromatography and asymmetric flow field-flow fractionation.* Cellulose, 2015. **22**(6): p. 3569-3581.

43. Vold, I.M.N. and B.E. Christensen, *Periodate oxidation of chitosans with different chemical compositions.* Carbohydrate Research, 2005. **340**(4): p. 679-684.

44. Gomez, C.G., M. Rinaudo, and M.A. Villar, *Oxidation of sodium alginate and characterization of the oxidized derivatives.* Carbohydrate Polymers, 2007. **67**(3): p. 296-304.

45. Painter, T.J., *Control of depolymerisation during the preparation of reduced dialdehyde cellulose.* Carbohydrate research, 1988. **179**: p. 259-268.

46. Kristiansen, K.A., A. Potthast, and B.E. Christensen, *Periodate oxidation of polysaccharides for modification of chemical and physical properties.* Carbohydrate Research, 2010. **345**(10): p. 1264-1271.

47. Liu, Y., et al., *Biodegradable natural pectin-based polysaccharide-gated low-voltage flexible oxide thin-film transistors for logic applications.* ACS Applied Electronic Materials, 2022. **4**(8): p. 4061-4067.

48. Cristescu, R., et al., *Matrix assisted pulsed laser evaporation processing of triacetate-pullulan polysaccharide thin films for drug delivery systems.* Applied Surface Science, 2006. **252**(13): p. 4647-4651.

49. Maver, T., et al., *Polysaccharide thin solid films for analgesic drug delivery and growth of human skin cells.* Frontiers in chemistry, 2019. **7**: p. 217.

50. Ahola, S., et al., *Model films from native cellulose nanofibrils. Preparation, swelling, and surface interactions.* Biomacromolecules, 2008. **9**(4): p. 1273-1282.

51. Wolfberger, A., et al., *Photolithographic patterning of cellulose: a versatile dual-tone photoresist for advanced applications.* Cellulose, 2015. **22**(1): p. 717-727.

52. Kontturi, E., T. Tammelin, and M. Österberg, *Cellulose—Model films and the fundamental approach.* Chemical Society Reviews, 2006. **35**(12): p. 1287-1304.

53. Seyrek, E. and G. Decher, *7.09 - Layer-by-layer assembly of multifunctional hybrid materials and nanoscale devices*, in *Polymer Science: A Comprehensive Reference*, K. Matyjaszewski and M. Möller, Editors. 2012, Elsevier: Amsterdam. p. 159-185.

54. Schaubeder, J.B., et al., *Xylan-cellulose thin film platform for assessing xylanase activity.* Carbohydrate Polymers, 2022. **294**: p. 119737.

55. Kittle, J.D., et al., *Equilibrium water contents of cellulose films determined via solvent exchange and quartz crystal microbalance with dissipation monitoring.* Biomacromolecules, 2011. **12**(8): p. 2881-2887.

56. Tammelin, T., et al., *Correlation between cellulose thin film supramolecular structures and interactions with water.* Soft Matter, 2015. **11**(21): p. 4273-4282.

57. Eronen, P., et al., *Interactions of structurally different hemicelluloses with nanofibrillar cellulose.* Carbohydrate Polymers, 2011. **86**(3): p. 1281-1290.

58. Mbam, S.O., et al., *Thin-film coating; historical evolution, conventional deposition technologies, stress-state micro/nano-level measurement/models and prospects projection: a critical review.* Materials Research Express, 2019. **6**(12): p. 122001.

59. Kontturi, E. and S. Spirk, *Ultrathin Films of Cellulose: A Materials Perspective.* Frontiers in Chemistry, 2019. **7**(488).

60. Meyerhofer, D., *Characteristics of resist films produced by spinning.* Journal of Applied Physics, 1978. **49**(7): p. 3993-3997.

61. Carmona, P., et al., *Structure formation and coarsening kinetics of phase-separated spin-coated ethylcellulose/hydroxypropylcellulose films.* Soft Matter, 2022. **18**(16): p. 3206-3217.

62. Carmona, P., et al., *Structure evolution during phase separation in spin-coated ethylcellulose/hydroxypropylcellulose films.* Soft Matter, 2021. **17**(14): p. 3913-3922.

63. Kargl, R., et al., *Functional patterning of biopolymer thin films using enzymes and lithographic methods.* Advanced Functional Materials, 2013. **23**(3): p. 308-315.

64. Siggia, E.D., *Late stages of spinodal decomposition in binary mixtures.* Physical Review A, 1979. **20**(2): p. 595-605.

65. Chesters, A.A., *The modelling of coalescence processes in fluid-liquid dispersions : a review of current understanding.* Chemical Engineering Research & Design, 1991. **69**: p. 259-270.

66. Hill, M.J. and P.J. Barham, *Ostwald ripening in polyethylene blends.* Polymer, 1995. **36**(17): p. 3369-3375.

67. Fleer, G., et al., *Polymers at interfaces*. 1993: Springer Science and Business Media.

68. Holmberg, K., B. Lindman, and B. Kronberg, *Surface chemistry of surfactants and polymers*. 2014: John Wiley & Sons.

69. Villares, A., et al., *Kinetic aspects of the adsorption of xyloglucan onto cellulose nanocrystals.* Soft Matter, 2015. **11**(32): p. 6472-6481.

70. Plunkett, M.A., et al., *Adsorption of pNIPAM layers on hydrophobic gold surfaces, measured in situ by QCM and SPR.* Langmuir, 2003. **19**(17): p. 6837-6844.

71. Albers, W.M. and I. Vikholm-Lundin, *Surface plasmon resonance on nanoscale organic films*, in *Nano-Bio-Sensing*. 2011, Springer. p. 83-125.

72. Naderi, A. and P.M. Claesson, *Adsorption properties of polyelectrolyte– surfactant complexes on hydrophobic surfaces studied by QCM-D.* Langmuir, 2006. **22**(18): p. 7639-7645.

73. Johannsmann, D., et al., *Viscoelastic properties of thin films probed with a quartz-crystal resonator.* Physical Review B, 1992. **46**(12): p. 7808-7815.

74. Merwe, P.A., *Surface plasmon resonance*. 2002. p. 1-4.

75. Khakalo, A., et al., *Using gelatin protein to facilitate paper thermoformability.* Reactive and Functional Polymers, 2014. **85**.

76. Saito, T., et al., *Cellulose nanofibers prepared by TEMPO-mediated oxidation of native cellulose.* Biomacromolecules, 2007. **8**(8): p. 2485-2491.

77. Theander, O. and E.A. Westerlund, *Studies on dietary fiber. 3. Improved procedures for analysis of dietary fiber.* Journal of Agricultural and Food Chemistry, 1986. **34**(2): p. 330-336.

78. Blumenkrantz, N. and G. Asboe-Hansen, *New method for quantitative determination of uronic acids.* Analytical Biochemistry, 1973. **54**(2): p. 484-489.

79. LeBel, R.G. and D.A.I. Goring, *Density, viscosity, refractive index, and hygroscopicity of mixtures of water and dimethyl sulfoxide.* Journal of Chemical & Engineering Data, 1962. **7**(1): p. 100-101.

80. Johnson, D., N. Hilal, and W.R. Bowen, *Chapter 1 - Basic principles of atomic force microscopy*, in *Atomic Force Microscopy in Process Engineering*, W.R. Bowen and N. Hilal, Editors. 2009, Butterworth-Heinemann: Oxford. p. 1-30.

81. Maekawa, E., T. Kosaki, and T. Koshijima, *Periodate oxidation of mercerized cellulose and regenerated cellulose*, in *Wood research : bulletin of the Wood Research Institute Kyoto University*. 1986, Wood Research Institute, Kyoto University. p. 44-49.

82. Leguy, J., et al., *Ultrastructural characterization of the core–shell structure of a wide range of periodate-oxidized cellulose from different native sources by solid-state 13C CP-MAS NMR.* ACS Sustainable Chemistry & Engineering, 2019. **7**(1): p. 412-420.

83. Wu, J., et al., *Influence of dialdehyde bacterial cellulose with the nonlinear elasticity and topology structure of ECM on cell adhesion and proliferation.* RSC Advances, 2014. **4**(8): p. 3998-4009.

84. Palasingh, C., et al., *Modification of xylan via an oxidation–reduction reaction.* Carbohydrate Polymers, 2022. **292**: p. 119660.

85. Simon, J., et al., *A fast method to measure the degree of oxidation of dialdehyde celluloses using multivariate calibration and infrared spectroscopy.* Carbohydrate Polymers, 2022. **278**: p. 118887.

86. Maekawa, E., *Analysis of oxidized moiety of partially periodate-oxidized cellulose by NMR spectroscopy.* Journal of Applied Polymer Science, 1991. **43**(3): p. 417-422.

87. Zhao, H. and N.D. Heindel, *Determination of degree of substitution of formyl groups in polyaldehyde dextran by the hydroxylamine hydrochloride method.* Pharmaceutical research, 1991. **8**(3): p. 400-402.

88. Chemin, M., et al., *Periodate oxidation of 4-O-methylglucuronoxylans: Influence of the reaction conditions.* Carbohydrate Polymers, 2016. **142**: p. 45-50.

89. Lyttle, D., E. Jensen, and W. Struck, *Simple volumetric assay for sodium borohydride.* Analytical Chemistry, 1952. **24**(11): p. 1843-1844.

90. Börjesson, M., et al., *Thermoplastic and flexible films from arabinoxylan.* ACS Applied Polymer Materials, 2019. **1**(6): p. 1443-1450.

91. Leguy, J., et al., *Periodate oxidation followed by NaBH4 reduction converts microfibrillated cellulose into sterically stabilized neutral cellulose nanocrystal suspensions.* Langmuir, 2018. **34**(37): p. 11066-11075.

92. Choulis, N.H., *49 - Miscellaneous drugs, materials, medical devices, and techniques*, in *Side Effects of Drugs Annual*, J.K. Aronson, Editor. 2012, Elsevier. p. 785-800.

93. Escalante, A., et al., *Flexible oxygen barrier films from spruce xylan.* Carbohydrate Polymers, 2012. **87**(4): p. 2381-2387.

94. Czibula, C., et al., *Design of friction, morphology, wetting, and protein affinity by cellulose blend thin film composition.* Frontiers in Chemistry, 2019. **7**(239).

95. Palasingh, C., et al., *Oxidized xylan additive for nanocellulose films – a swelling modifier.* International Journal of Biological Macromolecules, 2021. **180**: p. 753-759.